This is a preprint, the final version is subject to change, of the American Mineralogist (MSA)
Cite as Authors (Year) Title. American Mineralogist, in press.
(DOI will not work until issue is live.) DOI: http://dx.doi.org/10.2138/am-2015-5209

MANUSCRIPT 5209R – REVISION 1

Ankerite grains with dolomite cores: A diffusion chronometer for low- to medium-grade regionally metamorphosed clastic sediments

JOHN M. FERRY[1,*], JOANNE E. STUBBS[2], HUIFANG XU[3], YUNBIN GUAN[4] AND JOHN M. EILER[4]

[1]Department of Earth and Planetary Sciences, Johns Hopkins University, Baltimore, Maryland 21218, U.S.A.

[2]Center for Advanced Radiation Sources, University of Chicago, Chicago, Illinois 60637, U.S.A.

[3]Department of Geoscience, University of Wisconsin, Madison, Wisconsin 53706, U.S.A.

[4]Division of Geological and Planetary Sciences, California Institute of Technology, Pasadena, California 91125, U.S.A.

*E-Mail: jferry@jhu.edu

ABSTRACT

Ankerite grains with dolomite cores occur in marls, pelites, and psammites from a Buchan terrain in Maine and a Barrovian terrain in Vermont (U.S.A.). Dolomite cores are typically ≤20 μm in diameter, have sharp but irregular contacts with ankerite, and have the same crystallographic orientation as ankerite rims. Ankerite grains with dolomite cores are common in the chlorite zone, less abundant in the biotite and garnet zones, and rare (Vermont) or absent (Maine) at higher grades. The texture and crystallographic orientation of dolomite and ankerite and the sharpness of the dolomite-ankerite contact are consistent with partial replacement of detrital dolomite by ankerite by solution-reprecipitation. Metamorphic biotite is in Fe-Mg exchange equilibrium with ankerite rims but not with dolomite cores, implying that ankerite did not form long after biotite (biotite has no phlogopite cores). Possible sources of iron for the

formation of ankerite are reduction of ferric iron hydroxide or the smectite-to-illite reaction during diagenesis.

The sharpness of the dolomite-ankerite contact is a diffusion chronometer that constrains time scales of metamorphic process. Relatively low spatial resolution analyses of Fe/Mg across the contact with a NanoSIMS instrument and a FEG TEM give upper bounds on the thickness of the transition from ankerite to dolomite of ~2 μm and ~0.5 μm, respectively. Higher resolution analysis of BSE greyscale contrast with a FEG SEM gives a thickness ~100 nm. Fit of the greyscale profile to a model of one-dimensional diffusion across an infinite plane gives $Dt = 10^{-15}$ m^2 (± a factor of 5), where D is the effective Fe-Mg interdiffusion coefficient and t is the duration of diffusion. Using the published experimental determination of D, upper bounds on the residence time of ankerite grains with dolomite cores at peak T = 400 – 500 °C, on the duration of linear cooling from peak T to 100 °C, and on the duration of linear heating from 100 °C to peak T followed by linear cooling to 100 °C are all <1 year. For linear heating and cooling lasting 10^6 years, peak T could not have been >100 °C.

The question is what explains the occurrence of ultrasteep composition gradients between dolomite and ankerite. Regional metamorphism on a time scale of a year or less is unrealistic. No barrier to diffusion at the dolomite-ankerite contact was observed in TEM images. Post-metamorphic formation of ankerite at very low temperature is ruled out by Fe-Mg exchange equilibrium between biotite and ankerite but not dolomite. It is unlikely that the steep composition gradients were preserved by intracrystalline pressure gradients.

Alternatively, the steep composition gradients would be consistent with time scales of metamorphic process ~10^6 years or longer if D values during metamorphism were approximately six orders of magnitude or more smaller than those measured in the laboratory. The error of

measurement is much less, approximately ± a factor of 2. A correction to *D* for the difference in *P* between measurements (0.1 MPa) and metamorphism (350 – 800 MPa) is likely an order of magnitude or less. Oxygen activity (a_{O_2}), however, was 17 – 20 orders of magnitude larger during the laboratory measurements than during metamorphism. A correction to measured *D* for the difference in a_{O_2} between experiment and metamorphism appears to be the likeliest way to reconcile the steep composition gradients with realistic time scales of metamorphism. Before ankerite grains with dolomite cores are fully realized as a useful diffusion chronometer for low- and medium-grade metamorphic rocks, the rates of Fe-Mg interdiffusion in ankerite and dolomite need to be calibrated as a function of a_{O_2}.

INTRODUCTION

Arguably the least understood variable in igneous and metamorphic petrology is the duration of rock-forming processes. Building on the pioneering work of Lasaga (1983), however, there has been an increasing recognition over the last decade of the potential for intracrystalline compositional profiles to set rigorous upper limits on the duration that zoned crystals resided at the elevated temperatures at which rock-forming processes occurred (e.g., review by Mueller et al., 2010). The potential has been realized by recent precise laboratory measurements of the rates of intracrystalline cation diffusion in common minerals (e.g., review by Zhang and Cherniak, 2010), including, for example, garnet (Carlson, 2006; Borinski et al., 2012), olivine (Dohmen et al., 2007; Dohmen and Chakraborty, 2007), quartz (Cherniak et al., 2007), and clinopyroxene (Müller et al., 2013). In the study of volcanic igneous rocks, the inversion of measured intracrystalline composition profiles with fundamental equations governing diffusion and measured diffusion coefficients – diffusion chronometry – can set upper limits on the residence time of phenocrysts in a magma between the time when the phenocryst finished growth and the

time of eruption (e.g., Costa and Dungan, 2005; Saunders et al., 2012; Chamberlain et al., 2014). In the study of metamorphic rocks, diffusion chronometry sets upper limits on the duration that a metamorphic rock could have resided at the peak temperature of metamorphism, on the duration of cooling from peak temperature, and on the duration of heating and cooling (e.g., Ague and Baxter, 2007; Spear et al., 2012; Viete et al., 2011; Spear, 2014; Müller et al., 2015). The studies cited above have suggested surprisingly short time scales of igneous and metamorphic processes: a period as short as years to decades for the residence of phenocrysts in a magma prior to eruption and a period as short as $\sim 10^4 - 10^5$ years for residence of porphyroblasts at the peak temperature of regional metamorphism.

Intracrystalline composition gradients in metamorphic rocks suitable for diffusion chronometry, however, have not proved to be widespread. Furthermore, they have been mostly limited to date to medium- and high-grade regional metamorphic rocks that contain garnet, pyroxene, and quartz inclusions in garnet. A notable exception is the use of intracrystalline compositional variations in carbonate minerals to monitor short-duration events during contact metamorphism (Müller et al., 2008). What has been missing is the identification of features in low-grade regional metamorphic rocks that may serve as diffusion chronometers to complement studies of garnet, pyroxene, and quartz in medium- and high-grade rocks. In addition, such features would be ideal if they were widely distributed in regional metamorphic terrains so that constraints on duration of process could be derived over a range of spatial scales, rock types, and metamorphic grade. We report such a feature: the occurrence of ankerite grains with dolomite cores from regionally metamorphosed carbonates, pelites, and psammites from the chlorite, biotite, and garnet zones in northern New England, U.S.A. (Fig. 1). Because the rate of Fe-Mg interdiffusion in dolomite-ankerite solid solutions has been recently measured (Müller et al.,

2012), composition gradients between the dolomite cores and the ankerite rims can be quantitatively interpreted in terms of the duration of processes of regional metamorphism. Results, however, are unrealistic and point to a need for laboratory measurements of the rates of Fe-Mg interdiffusion in ankerite and dolomite over a greater range of oxygen activity with the goal of realizing the potential for this feature to serve as a useful diffusion chronometer for regionally metamorphosed rocks.

GEOLOGIC SETTING

A total of ~450 samples of ankerite-bearing rocks were examined in a Buchan terrain in south-central Maine and a Barrovian terrain in eastern Vermont. Lithologies represented include the metamorphosed equivalents of marls, pelites, psammites, and mafic and felsic igneous rocks. Grades of metamorphism (with reference to standard index minerals in pelitic schists) ranged from the chlorite zone to the staurolite-andalusite zone (Maine) or kyanite zone (Vermont).

Waterville-Vassalboro area, Maine

Approximately 100 samples of ankerite-bearing marl, pelite, and low-Al sulfide-rich schist were examined in the Waterville-Vassalboro area, Maine (Fig. 2). The geology of the area was established and extensively reviewed by Osberg (1968, 1979, 1988). Briefly, the Waterville and Vassalboro Formations are Silurian in depositional age. The Waterville Formation is largely composed of metamorphosed interbedded pelite, psammite, and minor marl. The Waterville limestone is a distinctive ~100-m thick member of the Waterville Formation that is almost all marl with rare schist interbeds (<1%). The Vassalboro Formation is mostly psammite with minor marl interbeds. Both formations were deformed and regionally metamorphosed during the Devonian Acadian Orogeny. The outcrop pattern of the Waterville limestone is defined by

isoclinally refolded recumbent folds. Osberg (1968 and personal communication) and Ferry (1984) mapped isograds in pelitic schists based on the development of biotite, garnet, staurolite + andalusite, and sillimanite during Buchan regional metamorphism. Porphyroblasts of biotite and amphibole in the Waterville limestone crosscut foliation parallel to the axial planes of the isoclinal folds. Metamorphism therefore post-dates almost all deformation. At high metamorphic grades, south of the area of Fig. 2, the Waterville and Vassalboro Formations were intruded by two granite plutons. Tucker et al. (2001) report a U-Pb zircon age of 378±1 Ma for the Togus pluton. The 364±3.5 Ma Th-Pb age of metamorphic monazite from pelites of the Waterville Formation (Wing et al., 2003) suggests that metamorphism was slightly younger than the plutonism. Based on mineral equilibria, *P* during metamorphism was ~350 MPa and *T* ranged from <400 °C in the chlorite zone to ~525 °C in the staurolite-andalusite zone.

Eastern Vermont

Approximately 350 samples of ankerite-bearing marl, pelite, psammite, and metaigneous rock were examined from the Waits River, Gile Mountain, and Albee Formations and from the Ammonoosuc Volcanics, mostly from the area in east-central Vermont illustrated in Fig. 3. The Waits River and Gile Mountain Formations are Siluro-Devonian in depositional age. The Waits River is composed of interbedded marl and pelite in variable proportions, and the Gile Mountain Formation is composed of psammite and pelite in variable proportions with minor marl interbeds (refer to Lyons, 1955; Doll et al., 1961; Hatch, 1988; and Hueber et al., 1990, and references therein for further details). The Albee Formation and Ammonoosuc Volcanics are Ordovician in depostional/extrusion age. Where sampled, the Albee Formation is composed of ~25% pelite, ~25% psammite, and ~50% mafic dikes. The Ammonoosuc Volcanics are composed of interlayered mafic and felsic volcanics rocks with minor interlayers of graphite-sulfide-rich

schist. All formations were folded and experienced Barrovian regional metamorphism during the Devonian Acadian orogeny (Thompson et al. 1968; Thompson and Norton 1968; Osberg et al. 1989). The areas sampled in the Albee Formation and the Amonoosuc Volcanics are far removed from the effects of the Ordovician Taconic orogeny in western Vermont. Mineral equilibria record P = 700-800 MPa during Devonian metamorphism and T increasing from ~450 °C at the biotite isograd in pelitic rocks to ~550 °C in the kyanite zone (Ferry, 1992, 1994; Menard and Spear 1993, 1994). For clarity, only the biotite and kyanite isograds are illustrated in Fig. 3.

METHODS OF INVESTIGATION

Almost all samples were collected as part of the first author's research over the last 40 years (Ferry, 1976, 1979, 1981, 1984, 1987, 1988, 1992, 1994; Penniston-Dorland and Ferry, 2006). An additional 21 samples of marl were collected specifically for this study from the Waits River Formation from five different roadcuts at location (**j**) in the inset to Fig. 3. Because ankerite grains with dolomite cores are undetectable in optical microscopy, all samples were examined for their presence or absence in polished thin sections by backscattered electron (BSE) microscopy with the JEOL JXA-8600 electron microprobe at Johns Hopkins University (JHU). Compositions of dolomite cores and ankerite rims were measured with the same instrument using wavelength-dispersive X-ray spectrometry with natural and synthetic mineral standards and a ZAF correction scheme (Armstrong, 1995).

Dolomite cores and the surrounding ankerite rims differ in composition primarily in X_{Fe} = Fe/(Fe+Mg) (determined by electron microprobe, Table 1). Compositional profiles at the contact between dolomite cores and ankerite rims, however, are too narrow to be accurately measured with an electron microprobe. Accordingly, composition profiles across dolomite-ankerite contacts were measured by three other techniques capable of finer spatial resolution. Contacts in

eleven grains from four marl samples (one from Maine and three from Vermont) were analyzed with the Cameca NanoSIMS 50L in the Division of Geological and Planetary Sciences at the California Institute of Technology. Because major elements were analyzed with an oxygen beam, the instrument was operated in the scanning mode with a beam diameter of ~700 nm. Profiles in Fe/Mg and Mn/Mg were retrieved from a 128x128 pixilated image of a 10-μm-square area across the contact by summing $^{56}Fe/^{26}Mg$ and $^{55}Mn/^{26}Mg$ ion intensity ratios of pixels in thin bands at right angles to a traverse perpendicular to the dolomite-ankerite contact in polished thin sections. The ion intensity ratios were converted to atomic Fe/Mg and Mn/Mg using an ankerite grain in the same section, previously analyzed by electron microprobe, as a standard. Analyses of ankerites with a range in X_{Fe} established a linear relationship with zero intercept between mass Fe/Mg and $^{56}Fe/^{26}Mg$ ion intensity ratios.

A foil for transmission electron microscope (TEM) analysis was extracted from one of the grains that had been analyzed by NanoSIMS, taken from one of the samples from Vermont. The grain was sub-sampled along a line perpendicular to the trace of the dolomite-ankerite contact using the FEI Nova 600 DualBeam SEM/focused ion beam (SEM/FIB) instrument in the Materials Research Science and Engineering Center (MRSEC), JHU. Images, selected area electron diffraction (SAED) patterns, and chemical analyses from the TEM foil were obtained using the Philips CM300 FEG TEM with SuperTwin lens operated at 300 kV in the Department of Earth and Planetary Sciences, JHU. Bright-field images were obtained in conventional TEM mode. Dark-field images and energy dispersive X-ray (EDS) analyses were obtained in the scanning TEM mode. The electron beam was defocused to a diameter of ~120 nm during EDS analysis to minimize beam damage. Measured Fe/Mg X-ray intensity ratios were converted to atomic Fe/Mg using a foil extracted from another ankerite grain in the same thin section,

previously analyzed by electron microprobe, that served as a standard. A simple proportionality between Fe/Mg and Fe/Mg X-ray intensity ratio was assumed.

Dolomite-ankerite contacts were examined with BSE microscopy in a polished thin section of a fourth sample from Vermont with the FEI 1500 CrossBeam FEG SEM/FIB in the Materials Sciences Center, University of Wisconsin, Madison, to perform analyses at a still finer spatial scale. The diameter of the electron beam was ~10 nm. Other studies have concluded that BSE greyscale level is a suitable proxy for X_{Fe} for the purposes of diffusion chronometry (e.g., Saunders et al., 2012; Chamberlain et al., 2014). Profiles in greyscale therefore were retrieved from pixilated images of the contact between a dolomite core and ankerite rim along traverses perpendicular to the contact at several positions along the contact.

ANKERITE WITH DOLOMITE CORES: OCCURRENCE AND PETROLOGIC CONTEXT

Occurrence and composition

Representative BSE images of the petrographic occurrence of ankerite grains with dolomite cores are reproduced in Fig 1. These include samples from Maine (Fig. 1a,b) and Vermont (Fig. 1c-f) and representative rocks types in which they are found: marl (Figs. 1a,c,d), pelite (Figs. 1b,f), and psammite (Fig. 1e). Dolomite cores are typically ≤~20 μm in diameter and are completely surrounded by ankerite rims. The contact between dolomite and ankerite is irregular but sharp at the scale of the images in Fig. 1. Quartz commonly occurs as inclusions in ankerite rims but never in dolomite cores. Dolomite cores do not occur in all ankerite-bearing rocks. In samples with dolomite cores, not every ankerite grain contains a dolomite core. In part, this is because the plane of the thin section does not intersect the center of all ankerite grains. When dolomite cores do occur, their abundance can vary widely between several grains and

several hundred grains in a 2.54 cm-diameter round thin section. The percentage of all ankerite grains in a sample that have dolomite cores also varies widely from one sample to another.

Dolomite and ankerite have compositions typical of those in metamorphic and sedimentary rocks with Ca ≥ (Mg+Fe+Mn) and Mg > Fe >> Mn (Table 1). The Ca content of dolomite is normally, but not always, slightly greater than in ankerite. Analyzed dolomite cores have very restricted compositions with $X_{Fe} \leq 0.03$ and <0.01 Mn atoms per formula unit (apfu). In contrast, analyzed ankerite rims have much more variable X_{Fe} ranging from 0.10 in marl sample 48-30-8 (Table 1; location (**j**), inset to Fig. 3) to 0.46 in pelite sample 411 (Fig. 2) and have Mn contents up to 0.05 apfu. Individual ankerite rims may either be uniform in composition or exhibit small spatial variations in X_{Fe}, as can be seen by examining enlargements of Fig. 1 for variations in BSE greyscale brightness.

The dolomite core and surrounding ankerite rim go to extinction simultaneously under crossed polarizers in optical microscopy, implying that the crystal lattices of dolomite and ankerite have the same orientation. This was confirmed by selected area electron diffraction (SAED) patterns obtained from dolomite and ankerite in the TEM foil that spans their mutual contact in one grain (see Appendix[1]). The SAED patterns demonstrate that orientations of the ankerite and dolomite crystal lattices are the same within error of measurement (± several degrees, given that the foil was slightly bent over its length). Bend contours were observed to ripple across the full length of the foil as the sample was tilted, indicating crystallographic continuity. Because carbonate minerals are highly susceptible to beam damage in the TEM, high-resolution transmission electron microscopy was not performed to determine whether the crystal lattices of dolomite and ankerite are continuous or not across their mutual contact.

[[1]Deposit item AM-15-xxxxx, Appendix. Deposit items are stored on the MSA web site and available via the American Mineralogist Table of Contents. Find the article in the table of contents at GSW (ammin.geoscienceworld.org) or MSA (www.minsocam.org), and then click on the deposit link.]

Petrologic Context

The petrologic context of ankerite grains with dolomite cores is summarized in Figs. 2 and 3. Symbols in both figures represent the locations where rocks with ankerite were examined. The different shapes of symbols denote different rock types. Filled symbols correspond to locations where at least one sample of a given rock type contains ankerite grains with dolomite cores; open symbols represent locations where all samples of a given rock type contain ankerite grains but none of the ankerite grains contain dolomite cores. Fractions identify locations where more than one sample of a given rock type was examined. The denominator indicates the total number of ankerite-bearing samples examined, and the numerator indicates how many of these contain ankerite grains with dolomite cores. Ankerite in all samples coexists with quartz and plagioclase; most samples additionally contain muscovite and calcite and many contain chlorite. The color of symbols refers to the presence or absence of biotite and calcic amphibole. Black symbols identify locations where all samples of a given rock type contain neither biotite nor calcic amphibole; red symbols refer to locations where at least one sample of a given rock type contains biotite but no calcic amphibole; green symbols (Fig. 3 only) identify locations where at least one sample of a given rock type contains calcic amphibole and biotite.

Ankerite grains with dolomite cores are more common in the chlorite zone than at higher grades in both Maine and Vermont. In Maine, ankerite grains with or without dolomite cores are absent from pelites in the biotite zone and at higher grades. Ankerite grains with dolomite cores

persist in marls into the biotite and garnet zones. Ankerite grains with or without dolomite cores are absent from marls in the high-grade portion of the garnet zone and at higher grades. With a single exception, carbonate rock samples examined from the Vassalboro Formation, both with and without biotite, contain abundant ankerite but no dolomite cores. All three samples of ankerite-bearing graphitic sulfide-rich schist contain ankerite grains with a dolomite core.

In contrast to Maine, ankerite grains with dolomite cores in Vermont persist in all clastic sedimentary rock types (marl, pelite, psammite) into the garnet zone. Also in contrast to Maine, ankerite occurs in marls, pelites, and psammites at grades higher than the garnet zone (i.e. the kyanite zone), but with the exception of two marl samples, the ankerite is devoid of dolomite cores. Dolomite cores are not observed in any of the ankerite-bearing marls from the kyanite zone that contain calcic amphibole. Ankerite grains in pelites and psammites from the kyanite zone do not contain dolomite cores. Metamorphosed igneous rocks from the Albee and Ammonoosucs Volcanics contain ankerite only in the chlorite zone, and the ankerite is devoid of dolomite cores.

Occurrences elsewhere

Although ankerite grains with dolomite cores are not commonly described in metamorphic rocks, they do occur elsewhere besides Maine and Vermont. Five samples of marl from the Wepawaug Schist, south-central Connecticut, U.S.A., kindly loaned by J. J. Ague, contain ankerite grains with dolomite cores. Ankerite grains with dolomite cores were noted in marls in the anchizone and epizone from the Central Swiss Alps by Livi et al. (2002).

FORMATION OF ANKERITE WITH DOLOMITE CORES

Mechanism of formation

Several potential explanations for the formation of ankerite grains with dolomite cores can be ruled out from textures (Fig. 1), mineral compositions (Table 1), and results of published laboratory experiments. Coexisting dolomite and ankerite cannot represent a solvus relationship for several reasons. First, laboratory experiments document continuous $Ca(Mg,Fe)(CO_3)_2$ solid solutions over the range in $X_{Fe} = 0.00 – 0.46$ exhibited by analyzed ankerite and dolomite in samples from Maine and Vermont (Goldsmith et al., 1962; Rosenberg, 1967). Second, dolomite is always completely surrounded by ankerite that isolates the dolomite from the other matrix grains. Coexisting discrete grains of dolomite and ankerite are never observed. Third, on textural grounds, dolomite cores are unlikely to have formed by exsolution from ankerite. Dolomite exsolved from calcite forms lamellae and small irregular blebs (e.g., Ferry et al., 2014) unlike the equant dolomite cores, some of which exhibit regular crystal faces (e.g., Figs. 1c,e,f). Fourth, while dolomite cores have almost the same composition, ankerite rims, even in samples from the same outcrop, have widely varying composition. For example, in 30 analyzed samples of marl from location 5 in the garnet zone of the Waterville Formation (Fig. 2), X_{Fe} of ankerite grains with dolomite cores varies between ~0.10 and ~0.20 (Fig. 4). The range in X_{Fe} illustrated in Fig. 4 is observed in ankerite in direct contact with dolomite cores. Considering that ankerite and dolomite from the outcrop are, for practical purposes, Fe-Mg solid solutions and assuming that temperature was uniform or nearly so during metamorphism over areas the size of the outcrop, a single X_{Fe} of ankerite in all samples is expected if ankerite and dolomite are related by a solvus.

Textural observations (Fig. 1) rule out the possibilities that ankerite is an overgrowth on unmodified detrital dolomite grains or that ankerite replaced dolomite by a process controlled by solid-state diffusion. Dolomite cores have angular, irregular shapes uncharacteristic of detrital grains. The transition between ankerite rim and dolomite core is much too narrow, in comparison

with the diameter of the ankerite grains, to be explained by replacement of dolomite by ankerite by intracrystalline Fe-Mg interdiffusion (see Fig. 6.1 of Crank, 1975).

The textures of the ankerite grains with dolomite cores in Fig. 1, on the other hand, are remarkably similar to those produced experimentally when a mineral crystal of one composition is replaced by one with a different composition by exchange of elements between the crystal and a coexisting aqueous fluid. An example is the replacement of albite by K-feldspar by exchange of K and Na between initial albite and coexisting K-bearing, initially Na-free, aqueous fluid (Niedermeier et al., 2009). If the exchange process is arrested, K-feldspar forms a rim around an unreplaced albite core. The contact between albite core and K-feldspar rim is sharp and irregular as are the contacts between dolomite and ankerite in Fig. 1. The crystal lattices of the unreplaced cores and replacement rims have the same orientation in both the products of the laboratory experiments with feldspar and in ankerite grains with dolomite cores. As will be demonstrated in a later section, in both experimental products and in ankerite rims, there can be a slight increase in the concentration of the introduced element (K in the experiments, Fe in ankerite) at the rim-core contact. The inferred mechanism of replacement in the experiments is solution-reprecipitation (Niedermeier et al., 2009). Because of the similarities in texture, crystallography, and composition between the experimental products and the ankerite rims around dolomite cores, the latter are inferred to have formed by incomplete replacement of dolomite by ankerite by a solution-reprecipitation mechanism as well. Replacement occurred by a Fe-Mg exchange reaction between original dolomite and fluid:

$$CaMg(CO_3)_2 + Fe^{2+} = CaFe(CO_3)_2 + Mg^{2+} \quad (1)$$

(the exact nature of the soluble Fe and Mg species is unimportant). Dolomite cores are exclusively observed in the metamorphosed equivalents of clastic sedimentary rocks (turbidites, according to Hatch, 1988). Prior to formation of ankerite rims, the original dolomite grains were likely detrital.

Timing of formation

The timing of the replacement of dolomite by ankerite is constrained by compositions of coexisting ankerite-biotite and ankerite-chlorite pairs (Fig. 5). Data in Fig. 5 for the Waterville and Waits River Formations are all from samples that contain ankerite with dolomite cores. The linear relationship between Fe/Mg of ankerite and both biotite and chlorite is consistent with a close approach to Fe-Mg exchange equilibrium between ankerite-biotite and ankerite-chlorite pairs. The slopes of the data arrays are the same within error of measurement as values obtained from larger data sets involving ankerite-biotite and ankerite-chlorite pairs from the Waterville and Waits River Formations (Penniston-Dorland and Ferry, 2006, their Table 3). No coexisting dolomite-phlogopite pairs are observed in the regional metamorphic rocks from Maine and Vermont. Fourteen dolomite-phlogopite pairs from four different contact aureoles, however, are plotted on Fig. 5a. Data for the contact metamorphic rocks prove that if biotite and chlorite equilibrated with dolomite rather than ankerite, their compositions would have been significantly Mg-richer than the intermediate Fe-Mg solid solutions observed in the regional metamorphic rocks.

Data in Fig. 5 are empirical evidence that biotite, produced during prograde regional metamorphism, attained Fe-Mg exchange equilibrium (or nearly so) with ankerite rims but not dolomite cores. The simplest explanation is that either ankerite rims were present and completely armored the dolomite cores at the time that biotite formed or that replacement of dolomite by

ankerite and formation of biotite were contemporaneous. There is no evidence that biotite initially crystallized as phlogopite and was later altered to a Fe-Mg solid solution (i.e., biotite does not contain phlogopite cores analogous to dolomite cores included in ankerite). Ankerite, therefore, could not have formed long after biotite. A complete post-metamorphic alteration of mineral compositions over such a large area and affecting such a wide range of rock types has never been documented in a regional metamorphic terrain and, if true, would have alarming implications for studies of metamorphic rocks.

Additional empirical evidence argues against contemporaneous formation of ankerite and biotite during metamorphism. First, the protoliths to biotite-bearing rocks in Maine and Vermont (i.e., rocks in the chlorite zone) contain ankerite but not biotite (Figs. 2, 3). Considering the concept of progressive metamorphism, ankerite formed first and biotite formed later at the expense of ankerite. Second, if replacement of dolomite by ankerite and formation of biotite occurred at the same time during metamorphism, either lower-grade protoliths contained a mineralogical reservoir of Fe^{2+} or the formation of ankerite and biotite involved spatially widespread iron metasomatism during metamorphism. Chlorite-zone marls that contain the required mineralogical reservoir of Fe^{2+} are not observed anywhere in northern New England, and regional scale iron metasomatism during metamorphism has never been documented anywhere. On the other hand, the commonplace formation of ankerite during diagenesis of sediments has been recognized for decades (e.g., Boles and Franks, 1979; Fisher and Land, 1986; Taylor and Sibley, 1986; Hendry et al., 2000; Parry et al., 2009). Formation of ankerite during diagenesis in rocks from Maine and Vermont prior to metamorphism makes more sense than formation of ankerite during metamorphism either from a Fe^{2+}-bearing reactant mineral that has never been observed or by metamorphic metasomatism that has never before been documented.

Source of iron

Replacement of dolomite by ankerite according to reaction 1 requires a source of soluble Fe^{2+}. Two sources are conceivable. The iron may have been introduced from an external source (i.e., iron metasomatism). Because ankerite likely formed during diagenesis, however, a more plausible source of iron is internal. In modern clastic sediments, much of the iron is deposited as ferric iron hydroxides, either crystalline or amorphous. Bacterial iron reduction during diagenesis converts solid ferric iron to dissolved ferrous iron by the reaction:

$$RM + 424\ Fe(OH)_3 + 848\ H^+ = 106\ CO_2 + 16\ NH_3 + H_3PO_4 + 424\ Fe^{2+} + 1166\ H_2O, \quad (2)$$

where "RM" is the Redfield molecule, $(CH_2O)_{106}(NH_3)_{16}(H_3PO_4)$, a simplified representation of organic matter (Taylor and Macquaker, 2011). Alternatively, Fe^{2+} in solution could have been produced internally by abiotic reduction of Fe^{3+} in smectite in the conversion of smectite to illite during diagenesis. The reduction of Fe^{3+} to soluble Fe^{2+} during the smectite-to-illite reaction has been demonstrated in the laboratory and is greatly accelerated by the presence of dissimilatory metal-reducing bacteria (Kim et al., 2004). Dissolved Fe^{2+} produced by reaction 2 or by the conversion of smectite to illite would then be available to drive reaction 1. Formation of ankerite during diagenesis can explain the occurrence of ankerite grains with dolomite cores in very low-grade metamorphic rocks from the anchizone (Livi et al., 2002). Different proportions of $Fe(OH)_3$ (or smectite) and dolomite in marl, psammite, and pelite sediments would further explain why X_{Fe} of ankerite varies widely in the range 0.10 – 0.46 in analyzed samples from this study.

DESTRUCTION OF DOLOMITE CORES

In Maine, ankerite, with or without dolomite cores, disappears from pelites exactly at the biotite isograd (Fig. 6) because ankerite (and dolomite cores, if present) was consumed by the biotite-forming reaction in pelites (Ferry, 1984). Ankerite, with or without dolomite cores, disappears from marls in the garnet zone (Fig. 6) because ankerite (and dolomite cores, if present) was consumed by reactions that formed biotite and calcic amphibole in marls in the garnet zone (Ferry, 1976, 1994). In Vermont, ankerite grains with dolomite cores disappear from pelites and psammites, as well as (with two exceptions) from marls, in the garnet zone. Ankerite without dolomite cores, however, commonly persists into the kyanite zone in all three lithologies (Fig. 6). The grain sizes of ankerite, calcite, and quartz are significantly larger in all rock types from the kyanite zone than in those from the chlorite zone where dolomite cores are common (Fig. 7). Dolomite cores were likely consumed in the kyanite zone by grain coarsening during prograde metamorphism. Grain coarsening probably occurred by a solution-reprecipitation mechanism that destroyed dolomite cores in the process and homogenized Fe and Mg in the original dolomite cores and ankerite rims.

CONSTRAINTS ON THE DURATION OF METAMORPHIC PROCESS FROM DIFFUSION CHRONOMETRY

Measurement of composition profiles across dolomite-ankerite contacts

To apply diffusion chronometry, composition profiles across dolomite-ankerite contacts were measured using three different instruments.

NanoSIMS analysis. Fe/Mg and Mn/Mg profiles were measured with a Cameca NanoSIMS 50L ion microprobe across dolomite-ankerite contacts in eleven grains from four samples of marl, three from Vermont and one from Maine. Figure 8a illustrates the location of analysis in one of the grains in sample 21-35D from the garnet zone of the Waits River

Formation (Fig. 3, Table 1). The measured Fe/Mg profile for the grain in sample 21-35D as well as for two of the other ten analyzed grains are illustrated in Figs. 8b-8d. Profiles of grains in one sample were irregular. In all other cases, the profiles were smooth with the apparent transition from dolomite to ankerite over ~2 μm. The smooth profiles were fit to an equation that describes one-dimensional diffusion perpendicular to a planar interface using a program provided by Daniel Vielzeuf (Vielzeuf et al., 2007). The fit assumes that the original composition profile was a perfect step function. Values of *Dt* retrieved from the Fe/Mg profiles are in the range $(1.5 – 4.0)\cdot10^{-13}$ m^2 (Fig. 8), where *D* is the effective intracrystalline diffusion coefficient and *t* is the duration of diffusion. Values of *Dt* were retrieved from both Mn/Mg and Fe/Mg profiles measured in the same grain from sample Q1j (not the same grain as in Fig. 1d), and they are $3.8\cdot10^{-13}$ m^2 and $2.5\cdot10^{-13}$ m^2, respectively. Results are consistent with the experimental evidence that Mn-Mg interdiffusion is slightly faster than Fe-Mg interdiffusion in ankerite and dolomite (Müller et al. (2012). Quantitatively the two measurements of *Dt* differ by a factor of 1.52, almost the same as a factor of 1.62 predicted from equations in Müller et al. (2012) for 475 °C, the inferred peak *T* of metamorphism at location Q1, Fig. 3 (Ferry, 2007).

Retrieved values of *Dt* are upper bounds both because the initial profile was assumed to have been a step function and because the profile may not have been exactly perpendicular to the dolomite-ankerite contact in three dimensions. Because the model $\sqrt{(Dt)}$ is slightly smaller than the ion beam diameter, the true value of *Dt* is likely smaller. Accordingly, the compositional profile across dolomite-ankerite contacts was measured with other instruments capable of higher spatial resolution.

EDS analysis by TEM. Fe/Mg profiles across the dolomite-ankerite contact in the grain in Fig. 8a were measured with a Philips CM300 FEG TEM. A TEM foil cut perpendicular to the

surface of the sample along the traverse perpendicular to the dolomite-ankerite contact in Fig. 8a is illustrated in Fig. 9a. Analyses were made along six traverses in the foil. Analyses along traverses 1 and 2 identified dolomite on the right-hand side and ankerite on the left-hand side of the foil and that ankerite and dolomite were uniform in composition within error of measurement away from their mutual contact. Analyses along traverses 3 and 4 were conducted to roughly locate the contact within the foil. Higher spatial resolution analyses were then made along traverses 5 and 6 perpendicular to the contact. Because the foil was cut vertically from a profile perpendicular to the dolomite-ankerite contact in thin section and because traverses 5 and 6 are perpendicular to the contact within the TEM foil, traverses 5 and 6 were perpendicular to the dolomite-ankerite contact in three dimensions. Analysis spots were separated by ~200 nm along traverse 5 and by ~170 nm along traverse 6. Results for traverses 5 and 6, illustrated in Fig. 9b, are nearly identical and confirm that the transition from dolomite to ankerite is narrower (~0.5 μm) than that indicated by NanoSIMS analysis. The profiles also reveal a slight enrichment of ankerite in Fe at the contact. By analogy with the experimental findings of Niedermeier et al. (2009), enrichment in Fe at the dolomite-ankerite contact is consistent with the conclusion that ankerite replaced dolomite by a solution-reprecipitation mechanism. Data for traverse 5 were fit to the same diffusion model assumed in the analysis of the NanoSIMS data (Fig. 9c). The fit omitted Fe/Mg values for ankerite > ~1 μm from the contact. As expected, the best-fit $Dt = 1.3 \cdot 10^{-14}$ m^2 is smaller than the values retrieved from the NanoSIMS data (Fig. 8b-d). The Dt value is also an upper bound because the initial profile may not have been a perfect step function. Because the model $\sqrt{(Dt)}$ is slightly smaller than the electron beam diameter, the true value of Dt was likely smaller. Accordingly, the compositional profile across one dolomite-ankerite contact was measured with other instrumentation that attains yet higher spatial resolution.

BSE greyscale analysis by SEM. BSE greyscale profiles were measured in three places perpendicular to the dolomite-ankerite contact within a single grain in sample 21-35I (Fig. 1c) with a FEI 1500 CrossBeam FEG SEM/FIB. Sample 21-35I is from the same carbonate layer as sample 21-35D from which NanoSIMS and TEM profiles were obtained. Representative results (Fig. 9d) confirm expectations that the transition from dolomite to ankerite (~100 nm) is narrower than indicated by EDS analysis using the TEM. A fit of the greyscale data to the diffusion model returns a yet smaller value of $Dt = 1.2 \cdot 10^{-15}$ m^2. Because of the scatter in the greyscale values, the uncertainty in the Dt was estimated by computing upper and lower bounds that bracket most of the data over the transition from dolomite to ankerite. The brackets (dashed red curves, Fig. 9d) correspond to an uncertainty in Dt of approximately a factor of five. Because $\sqrt{(Dt)}$ is greater than the electron beam diameter, the Dt value from the greyscale profile is preferred over values obtained by NanoSIMS and TEM analysis. Even $Dt = 1.2 \cdot 10^{-15}$ m^2, however, is an upper bound because the profile is not likely to have been perpendicular to the dolomite-ankerite contact in three dimensions and because the initial profile may not have been a perfect step function.

Constraints on the duration of metamorphic processes

Using experimentally-determined values of D (D_{exp}) from Müller et al. (2012), measured values of Dt [$(Dt)_{meas}$] constrain the duration of various metamorphic processes. Peak metamorphic temperatures (T_{peak}) used in the calculations, 400-500 °C, are those recorded by mineral equilibria and reported in an earlier studies (Ferry, 1992, 1994, 2007). Calculations using 400 °C as the value of T_{peak} are conservative because 400 °C is 50-100 °C lower than estimated values of T_{peak} for the samples in which Fe/Mg profiles were measured. It is unlikely that estimated values of T_{peak} err by >50-100 °C. Results are listed in Table 3.

Residence time at peak temperature. An upper bound on the time that analyzed ankerite grains with dolomite cores could have resided at peak temperature is $(Dt)_{meas}/(D_{exp})$ with (D_{exp}) computed for 400 °C and 500 °C from the relevant equation in Müller et al. (2012). Durations range from 0.1 years derived from the greyscale data with T_{peak} = 500 °C to 60 years for the largest value of $(Dt)_{meas}$ measured by NanoSIMS with T_{peak} = 400 °C. These are upper bounds because the calculations ignore the time required to heat the sample to peak temperature and to cool it back to ambient conditions and because the values of $(Dt)_{meas}$ are upper bounds.

Linear cooling time from peak temperature. An upper bound on the time that analyzed grains cooled linearly from peak temperature to 100 °C is $(Dt)_{meas}/(D_{eff})$ where D_{eff} is the effective value of D during cooling, computed from:

$$D_{\text{eff}} = \left[\int_{100}^{T_{\text{peak}}} D_{\text{exp}}(T)\,\mathrm{d}T \right] / (T_{\text{peak}} - 100) \quad (3)$$

(the exact lower limit of integration is unimportant). Durations of cooling range from 0.3 years derived from the greyscale data with T_{peak} = 500 °C to 210 years for the largest value of $(Dt)_{meas}$ measured by NanoSIMS with T_{peak} = 400 °C. These are upper bounds because the calculations ignore the time required to heat the sample to peak temperature and because the values of $(Dt)_{meas}$ are upper bounds.

Linear heating and cooling time to and from peak temperature. Estimates of the time that analyzed grains heated linearly from 100 °C to peak temperature and then immediately cooled linearly back to 100° C are identical to durations of linear cooling because the effects of heating and cooling on mass transport by diffusion are identical. Estimates are also upper bounds because the values of $(Dt)_{meas}$ are upper bounds.

Peak temperature for linear cooling over 10^6 years. Using values of $(Dt)_{meas}$ and Equation 3, the value of T_{peak} that returns a linear cooling time of 10^6 years can be computed. That value of T_{peak} is <100 °C for values of $(Dt)_{meas}$ measured by each of the three methods.

PRESERVATION OF STEEP COMPOSITION GRADIENTS AT DOLOMITE-ANKERITE CONTACTS

The question is what explains the occurrence of ultrasteep composition gradients between dolomite and ankerite in regionally metamorphosed clastic sediments from northern New England. There are numerous possible answers, all but one of which seem implausible. Setting aside the values of $(Dt)_{meas}$ derived from the NanoSIMS data that are demonstrably too large (because of the relatively large beam size used), the steep compositional gradients could be preserved if the entire cycle of regional metamorphism including heating, residence time at T_{peak}, and cooling lasted no more than a few years or if T_{peak} < 100 °C. Neither possibility is remotely in the realm of current understanding of time scales and peak temperatures of regional metamorphism (England and Thompson, 1984; Ague and Baxter, 2007; Viete et al., 2011).

The steep compositional gradients between dolomite cores and ankerite rims may be preserved because there is some barrier to diffusion at their mutual contact, like a gap or a precipitate of another mineral. Examination of one contact with TEM (Fig. 9a), however, failed to reveal any such unusual feature, although numerous defects were observed arranged in lines (likely planes in three dimensions) within dolomite parallel to the contact. Furthermore, the composition profiles measured by TEM show equally steep (albeit shorter) compositional gradients entirely within ankerite (Fig. 9b). Steep intracrystalline compositional profiles entirely within ankerite have the same implication for short durations of peak *T*, heating, and cooling during metamorphism as do the steep composition profiles across the dolomite-ankerite contacts but without the complication of a possible barrier to diffusion across the contact.

Steep compositional gradients at dolomite-ankerite contacts could be preserved if iron metasomatism and replacement of dolomite by ankerite occurred at very low temperature following regional metamorphism. Alternatively, ankerite rims might somehow be the result of late, low-temperature retrograde dynamic recrystallization with dolomite representing undeformed and unrecrystallized porphyroclastic cores (e.g., Ashley et al., 2014). In either case, the temperature of replacement or recrystallization, however, would have had to be <100 °C. Even for replacement of dolomite by ankerite and then residence at 100 °C, the measured Fe/Mg profiles across the dolomite-ankerite contact would not survive longer than 10^6 years. It is unclear how replacement or recrystallization at such low temperatures could also change the compositions of biotite and chlorite without at the same time altering those minerals to low-temperature sheet silicates. The possibility of a low-temperature replacement or recrystallization process that completely and pervasively changes the compositions that minerals in metamorphic rocks once had during metamorphism over areas of 1000s of km^2 is also far removed from the realm of current understanding of metamorphism.

Our understanding of the relationships among lithostatic pressure, stress, mineral assemblages, and mineral compositions during regional metamorphism is currently being questioned (Schmalholz and Podladchikov, 2014; Tajcmanova et al., 2014; Wheeler, 2014). It is possible that the steep compositional gradients at dolomite-ankerite contacts were preserved by local pressure or stress gradients. Following the analysis of Tajcmanova et al. (2014), the differences in composition between dolomite cores and ankerite rims in the samples listed in Table 1 could be maintained at peak temperature by pressure differences of 1.1 – 1.6 GPa (using molar volumes calculated from Holland and Powell, 1998, and activities of $CaMg(CO_3)_2$ and $CaFe(CO_3)_2$ calculated from the current version of their AX program). The estimated pressure

differences are questionable given that the pressure of metamorphism in Maine and Vermont, estimated from mineral equilibria, is ~350 MPa and 700 – 800 MPa, respectively. In addition, the mechanical model of Tajcmanova et al. (2014), that forms the basis for the calculations of pressure differences, considers a higher-density mineral included in a lower-density host. Dolomite, however, is less dense than ankerite, and the calculations predict the puzzling result that dolomite cores would have had to be at a pressure 1.1 – 1.6 GPa less than surrounding ankerite to preserve the measured composition gradients.

On the other hand, the steep composition gradients at dolomite-ankerite contacts require no special mechanism of preservation if the values of D used in the calculations of time scales of metamorphic process in Table 3 somehow are in error. In order to retrieve more reasonable heating and cooling times on the order of 10^6 years or more from the measured composition gradients at dolomite-ankerite contacts, values of D would have to be smaller than those measured by Müller et al. (2012) by at least six orders of magnitude. Their stated uncertainty in individual measurements of D_{exp} is much smaller, however, approximately ± a factor of 2.

The laboratory experiments of Müller et al. (2012) did not investigate the possible dependence of the rate of Fe-Mg interdiffusion on crystal orientation. There is no measurable dependence of the rate of Ca diffusion in calcite on crystal orientation (Farver and Yund, 1996), and diffusion of Fe and Mg in ankerite and dolomite may be similar. An absence of significant orientation-dependent diffusion of Fe and Mg is independently supported by a steepness of the compositional gradient at dolomite-ankerite contacts that does not visibly vary within grains (Fig. 1) or between grains in the same thin section. It seems unlikely, therefore, that the unreasonably short time scales of metamorphism in Table 3 are an artifact of D values that vary by six orders of magnitude in ankerite and dolomite as a function of crystal orientation.

Values of D used in the calculations of times scales of metamorphism may err because of the difference in P between the experiments of Müller et al. (2012) and metamorphism in Maine and Vermont was not accounted for. Pressure during the measurements of D_{exp} was 0.1 MPa; P during metamorphism in Maine and Vermont was ~350 MPa and ~700 – 800 MPa, respectively. Increasing P slows diffusion of Fe and Mg in olivine (Dohmen et al., 2007; Dohmen and Chakraborty, 2007), in garnet (Carlson, 2006), and presumably also in ankerite and dolomite. The P-dependence of the rate of diffusion of Fe and Mg in olivine and garnet, however, is small; in both cases, a change in P from 0.1 MPa to 350-800 MPa is predicted to lower D by <1 log unit. Dolomite-ankerite solid solutions are not likely to behave significantly differently. The difference in P between experiment and metamorphism therefore seems inadequate to provide the correction in D needed to retrieve time scales on the order of 10^6 years or longer from the composition profiles across dolomite-ankerite contacts.

Finally, values of D used to calculate the short time scales of metamorphism in Table 3 may err because the difference in oxygen activity (a_{O_2}) between the experiments of Müller et al. (2012) and metamorphism in Maine and Vermont was not accounted for. In the experiments, a_{O_2} was set by the equilibrium associated with dissociation of CO_2 by

$$2\ CO_2 = 2\ CO + O_2, \quad (4)$$

with $a_{CO_2} \approx 1$ in the nominally pure CO_2 fluid and $a_{CO} = 2a_{O_2}$ (Fig. 10). Graphite is ubiquitous in the samples of metamorphosed marl, pelite, and psammite examined from Vermont and Maine. In contrast, therefore, a_{O_2} during metamorphism in Maine and Vermont was set by the graphite-CO_2 equilibrium,

$$C + O_2 = CO_2, \quad (5)$$

in the presence of CO_2-H_2O fluid. In the biotite and garnet zones in Maine and Vermont where peak *T* was in the range 400 – 500 °C, $a_{CO_2}$was 0.099 – 0.362, based on the equilibrium,

$$\underset{\text{muscovite}}{KAl_3Si_3O_{10}(OH)_2} + 3\ \underset{\text{ankerite}}{CaMg(CO_3)_2} + 2\ \underset{\text{quartz}}{SiO_2} =$$

$$\underset{\text{biotite}}{KMg_3AlSi_3O_{10}(OH)_2} + \underset{\text{plagioclase}}{CaAl_2Si_2O_8} + 2\ \underset{\text{calcite}}{CaCO_3} + 4\ \underset{\text{fluid}}{CO_2} \qquad (6)$$

(Penniston-Dorland and Ferry, 2006; Ferry, 2007, 2015). Calculated a_{O_2} during metamorphism, accordingly, was 17 – 20 orders of magnitude less than in the experiments (Fig. 10).

One way to represent the dependence of *D* on redox state is in terms of the ratio of the fugacity of O_2 (f_{O_2}) at *P* and *T* of interest to f_{O_2} in a reference state at the same *P* and *T* (e.g., Carlson, 2006). The difference in the logarithm of this fugacity ratio between two states of interest is identical to the difference in the logarithm of a_{O_2} between the two states. Accordingly, Carlson's (2006) model predicts that decreasing a_{O_2} slows Fe-Mg interdiffusion in garnet with changes in log*D* scaling with (1/6) changes in loga_{O_2}. The relation between log*D* and loga_{O_2} or logf_{O_2} for other Fe-Mg minerals, however, can be different and more complicated (e.g., Dohmen and Chakraborty, 2007; Müller et al., 2013; Vogt et al., 2015). The correction of *D* for a_{O_2} in Fe-Mg dolomite and ankerite solid solutions is not known. Nevertheless, the tentative conclusion is that the unreasonably short time scales of metamorphism in Table 3 are likely an artifact of the failure to correct *D* values for the 17 – 20 orders of magnitude difference in a_{O_2} between the experiments of Müller et al. (2012) and the conditions of regional metamorphism in Maine and Vermont. If correct, the preservation of sharp compositional gradients at dolomite-ankerite

contacts then is explained by the relatively low a_{O_2} of graphite-bearing rocks during metamorphism (Fig. 10). This explanation, of course, begs for further laboratory experiments that will lead to a quantitative understanding of the dependence of D on a_{O_2} for ankerite and dolomite solid solutions.

IMPLICATIONS

Ultrasteep composition gradients at contacts between dolomite cores and surrounding ankerite rims in regional metamorphic rocks are spatially widespread and occur in a variety of common rock types and in different environments and grades of metamorphism. Ankerite grains with dolomite cores, therefore, potentially can serve as an extraordinarily useful diffusion chronometer for metamorphic processes in low- and medium-grade rocks. The potential, however, will only be fully realized when new experiments calibrate the effect of a_{O_2} (and additionally the lesser effect of P) on the rate of Fe-Mg interdiffusion in dolomite and ankerite.

ACKNOWLEDGMENTS

Research supported by NSF grants EAR-0635608 and EAR-1118713 to JMF; by U. S. Department of Energy, Basic Energy Sciences grant DE-FG02-89ER14074 to JES; and NASA Astrobiology Institute grant N07-5489 to HX. We thank Kyle Ashley and Lukas Baumgartner for their thoughtful and constructive reviews. Tim Holland kindly calculated the oxygen fugacities used to construct Fig. 10.

REFERENCES

Ague, J.J., and Baxter, E.F. (2007) Brief thermal pulses during mountain building recorded by Sr diffusion in apatite and multicomponent diffusion in garnet. Earth and Planetary Science Letters, 261, 500-516.

Armstrong, J.T. (1995) CITZAF: a package of correction programs for the quantitative correction of microbeam X-ray analysis of thick polished materials, thin films, and particles. Microbeam Analysis, 4, 177-200.

Ashley, K.T., Carlson, W.D., Law, R.D., and Trace, R.J. (2014) Ti resetting in quartz during dynamic recrystallization: Mechanisms and significance. American Mineralogist, 99, 2025-2030.

Boles, J. R. and Franks, S. G. (1979) Clay diagenesis in Wilcox sandstones of southwest Texas: Implications of smectite diagenesis on sandstone cementation. Journal of Sedimentary Petrology, 49, 55-70.

Borinski, S.A., Hoppe, U., Chakraborty, S., Ganguly, J., and Bhowmik, S.K. (2012) Multicomponent diffusion in garnets I: general theoretical considerations and experimental data for Fe-Mg systems. Contributions to Mineralogy and Petrology, 164, 571-586.

Carlson, W.D. (2006) Rates of Fe, Mg, Mn, and Ca diffusion in garnet. American Mineralogist, 91, 1-11.

Chamberlain, K.J., Morgan, D.J., and Wilson, C.J.N. (2014) Timescales of mixing and mobilisation in the Bishop Tuff magma body: perspectives from diffusion chronometry. Contributions to Mineralogy and Petrology, 168, 1034-1056.

Cherniak, D.J., Watson, E.B., and Wark, D.A. (2007) Ti diffusion in quartz. Chemical Geology, 236, 65-74.

Costa, F., and Dungan, M. (2005) Short time scales of magmatic assimilation from diffusion modeling of multiple elements in olivine. Geology, 33, 837-840.

Crank, J. (1975) The Mathematics of Diffusion. Oxford University Press, Oxford.

Davis, S.R., and Ferry, J.M. (1993). Fluid infiltration during contact metamorphism of interbedded marble and calc-silicate hornfels, Twin Lakes area, central Sierra Nevada, California. Journal of Metamorphic Geology**,** 11, 71-88.

Dohmen, R., Becker, H.-W., and Chakraborty, S. (2007) Fe-Mg diffusion in olivine I: experimental determination between 700 and 1,200 °C as a function of composition, crystal orientation and oxygen fugacity. Physics and Chemistry of Minerals, 34, 389-407.

Dohmen, R., and Chakraborty, S. (2007) Fe-Mg diffusion in olivine II: point defect chemistry, change of diffusion mechanisms and a model for calculation of diffusion coefficients in natural olivine. Physics and Chemistry of Minerals, 34, 409-430.

Doll, C.G., Cady, W.M., Thompson, J.B., Jr., and Billings, M.P., compilers and Eds. (1961) Centennial Geologic Map of Vermont. Vermont Geologic Survey, Montpelier.

England, P.C., and Thompson, A.B. (1984) Pressure-temperature-time paths of regional metamorphism I. Heat transfer during the evolution of thickened continental crust. Journal of Petrology, 25, 894-928.

Farver, J.R., and Yund, R.A. (1996) Volume and grain boundary diffusion of calcium in natural and hot-pressed calcite aggregates. Contributions to Mineralogy and Petrology, 123, 77-91.

Ferry, J.M. (1976) Metamorphism of calcareous sediments in the Waterville-Vassalboro area, south-central Maine: mineral reactions and graphical analysis. American Journal of Science, 276, 841-882.

_____ (1979) A map of chemical potential differences within an outcrop. American Mineralogist, 64, 966-985.

_____ (1981) Petrology of graphitic sulfide-rich schists from south-central Maine: an

example of desulfidation during prograde regional metamorphism. American Mineralogist, 66, 908-930.

_____ (1984) A biotite isograd in south-central Maine, U.S.A.: mineral reactions, heat transfer, and fluid transfer. Journal of Petrology, 25, 871-893.

_____ (1987) Metamorphic hydrology at 13-km depth and 400-550 °C. American Mineralogist, 72, 39-58.

_____ (1988) Infiltration-driven metamorphism in northern New England, USA. Journal of Petrology, 29, 1121-1159.

_____ (1992) Regional metamorphism of the Waits River Formation, eastern Vermont: delineation of a new type of giant metamorphic hydrothermal system. Journal of Petrology, 33, 45-94.

_____ (1994) Overview of the petrologic record of fluid flow during regional metamorphism in northern New England. American Journal of Science, 294, 905-988.

_____ (1996) Prograde and retrograde fluid flow during contact metamorphism of siliceous carbonate rocks from the Ballachulish aureole, Scotland. Contributions to Mineralogy and Petrology, 124, 235-254.

_____ (2007) The role of volatile transport by diffusion and dispersion in driving biotite-forming reactions during regional metamorphism of the Gile Mountain Formation, Vermont. American Mineralogist, 92, 1288-1302.

_____ (2015) Fluids in the crust during regional metamorphism: Forty years in the Waterville limestone. American Mineralogist, 100, in press.

Ferry, J.M., and Rumble D., III (1997) Formation and destruction of periclase by fluid flow in two contact aureoles. Contributions to Mineralogy and Petrology, 128, 313-334.

Ferry J.M., Sorensen, S.S., and Rumble D., III (1998) Structurally controlled fluid flow during contact metamorphism in the Ritter Range pendant, California, USA. Contributions to Mineralogy and Petrology, 130, 358-378.

Ferry, J.M., Kitajima, K., Strickland, A., and Valley, J.W. (2014) Ion microprobe survey of the grain-scale oxygen isotope geochemistry of minerals in metamorphic rocks. Geochimica et Cosmochimica Acta, 144, 403-433

Fisher, R. S., and Land, L. S. (1986) Diagenetic history of Eocene Wilcox sandstones, South-Central Texas. Geochimica et Cosmochimica Acta, 50, 551-561.

Goldsmith, J.R., Graf, D.L., Witters, J., and Northrup, D.A. (1962) Studies in the system $CaCO_3$-$MgCO_3$-$FeCO_3$: 1. Phase relations; 2. A method for major-element spectrochemical analysis; 3. Compositions of some ferroan dolomites. Journal of Geology, 70, 659-688.

Hatch, N.L., Jr. (1988) Some revisions to the stratigraphy and structure of the Connecticut Valley trough, eastern Vermont. American Journal of Science, 288, 1041-1059.

Hendry, J. P., Wilkinson, M., Fallick, A. E., and Haszeldine, R. S. (2000) Ankerite cementation in deeply buried Jurassic sandstone reservoirs of the central North Sea. Journal of Sedimentary Research, 70, 227-239.

Holland, T.J.B., and Powell, R. (1998) An internally consistent thermodynamic data set for phases of petrological interest. Journal of Metamorphic Geology, 16, 309-343.

_____ (1991) A Compensated-Redlich-Kwong (CORK) equation for volumes and fugacities of CO_2 and H_2O in the range 1 bar to 50 kbar and 100-1600 °C. Contributions to Mineralogy and Petrology, 109, 265-273.

Hueber, F.M., Bothner, W.A., Hatch, N.L., Jr., Finney, S.C., and Aleinikoff, J.N. (1990)

Devonian plants from southern Quebec and northern New Hampshire and the age of the Connecticut Valley trough. American Journal of Science**,** 290, 360-395.

Kim, J., Dong, H., Seabaugh, J., Newell, S.W., and Eberl, D.S. (2004) Role of microbes in the smectite-to-illite reaction. Science, 303, 830-832.

Lasaga, A. C. (1983) Geospeedometry: An extension of geothermometry. In S. K. Saxena, Ed., Kinetics and Equiloibrium in Mineral Reactions, p. 81-114. Springer-Verlag, New York.

Livi, K.J.T., Ferry, J.M., Veblen, D.R., Frey, M., and Connolly, J.A.D. (2002) Reactions and physical conditions during metamorphism of Liassic aluminous black shales and marls in central Switzerland. European Journal of Mineralogy, 14, 647-672.

Lyons, J.B. (1955) Geology of the Hanover quadrangle, New Hampshire-Vermont. Geological Society of America Bulletin, 66, 105-146.

Menard, T. and Spear, F.S. (1993) Metamorphism of calcic pelitic schists, Strafford Dome, Vermont: compositional zoning and reaction history. Journal of Petrology, 34, 977-1005.

_____ (1994) Metamorphic P-T paths from calcic pelitic schists from the Strafford Dome, Vermont, USA. Journal of Metamorphic Geology, 12, 811-826.

Mueller, T., Watson, E.B., and Harrison, T.M. (2010) Applications of diffusion data to high-temperature Earth systems. In Y. Zhang and D.J. Cherniak, Eds., Diffusion in Minerals and Melts, 72, p. 997-1038. Reviews in Mineralogy and Geochemistry, Mineralogical Society of America, Chantilly, Virginia.

Müller, T., Baumgartner, L.P., Foster, C.T., Jr., and Roselle, G.T. (2008) Forward modeling of the effects of mixed volatile reaction, volume diffusion, and formation of submicroscopic exsolution lamellae in calcite-dolomite thermometry. American Mineralogist, 93, 1245-1259.

Müller, T., Cherniak, D., and Watson, E.B. (2012) Interdiffusion of divalent cations in carbonates: experimental measurements and implications for timescales of equilibration and retention of compositional signatures. Geochimica et Cosmochimica Acta, 84, 90-103.

Müller, T., Dohmen, R., Becker, H.W., ter Heege, J.H., and Chakraborty, S. (2013) Fe-Mg interdiffusion rates in clinopyroxene: experimental data and implications for Fe-Mg exchange geothermometers. Contributions to Mineralogy and Petrology, 166, 1563-1576.

Müller, T., Massonne, H.-J., and Willner, A.P. (2015) Timescales of exhumation and cooling inferred by kinetic modelling: An example using lamellar garnet pyroxenite from the Variscan Granulitgebirge, E Germany. American Mineralogist, 100, 747-759.

Niedermeier, D.R.D., Putnis, A., Geisler, T., Golla-Schindler, U., and Putnis, C.V. (2009) The mechanism of cation and oxygen isotope exchange in alkali feldspars under hydrothermal conditions. Contributions to Mineralogy and Petrology, 157, 65-76.

Osberg, P.H. (1968) Stratigraphy, structural geology, and metamorphism in the Waterville-Vassalboro area, Maine. Maine Geological Survey Bulletin 20.

_____ (1979) Geologic relationships in south-central Maine. In P.H. Osberg and J.W. Skehan, Eds. The Caledonides in the U.S.A., p. 37-62. Weston Observatory of Boston College, Weston, Massachusetts.

_____ (1988) Geologic relations in the shale-wacke sequence in south-central Maine. Maine Geological Survey Studies in Maine Geology, 1, 51-73

Osberg, P.H., Tull, J.F., Robinson, P., Hon, R., and Butler, J.R. (1989) The Acadian orogen. In

R.D. Hatcher, Jr., W.A. Thomas, and G.W. Viele, Eds., The Appalachian-Ouachita Orogen in the United States. The Geology of North America, F-2, p. 179-232. Geological Society of America, Boulder.

Parry, W. T., Chan, M. A., and Nash, B. P. (1986) Diagenetic characteristics of the Jurassic Navaho Sandstone in the Covenant oil field, central Utah thrust belt. American Association of Petroleum Geologists Bulletin, 93, 1039-1061.

Penniston-Dorland, S.C., and Ferry, J.M. (2006) Development of spatial variations in reaction progress during regional metamorphism of micaceous carbonate rocks, northern New England. American Journal of Science, 306, 475-524.

Rosenberg, P.E. (1967) Subsolidus relations in the system $CaCO_3$-$MgCO_3$-$FeCO_3$ between 350 ° and 550 °C. American Mineralogist, 52, 787-796.

Saunders, K., Blundy, J., Dohmen, R., and Cashman, K. (2012) Linking petrology and seismology at an active volcano. Science, 336, 1023-1027.

Schmalholz, S.M., and Podladchikov, Y. (2014) Metamorphism under stress: the problem of relating minerals to depth. Geology, 42, 733-734.

Spear, F.S. (2014) The duration of near-peak metamorphism from diffusion modelling of garnet zoning. Journal of Metamorphic Geology, 32, 903-914.

Spear, F.S., Ashley, K.T., Webb, L.E., and Thomas, J.B. (2012) Ti diffusion in quartz inclusions: Implications for metamorphic time scales. Contributions to Mineralogy and Petrology, 164, 977-986.

Tajcmanova, L., Podladchikov, Y., Powell, R., Moulas, E., Vrijmoed, J.C., and Connolly, J.A.D. (2014) Grain-scale pressure variations and chemical equilibrium in high-grade metamorphic rocks. Journal of Metamorphic Geology, 32, 195-207.

Taylor, K.G., and Macquaker, J.H.S. (2011) Iron minerals in marine sediments record chemical environments. Elements, 7, 113-118.

Taylor, T. R., and Sibley, D. F. (1986) Petrographic and geochemical characteristics of dolomite types and the origin of ferroan dolomite in the Trenton Formation, Ordovician, Michigan Basin, U.S.A., Sedimentology, 33, 61-86.

Thompson, J.B., Jr., and Norton, S.A. (1968) Paleozoic regional metamorphism in New England and adjacent areas. In E-an Zen, W.S. White, J.B. Hadley, and J.B. Thompson, Jr., Eds., Studies of Appalachian Geology: Northern and Maritime, p. 319-317. John Wiley and Sons, New York.

Thompson, J.B., Jr., Robinson, P., Clifford, T.N., and Trask, N.J., Jr. (1968) Nappes and gneiss domes in west-central New England. In E-an Zen, W.S. White, J.B. Hadley, and J.B. Thompson, Jr., Eds., Studies of Appalachian Geology: Northern and Maritime, p. 203-218. John Wiley and Sons, New York.

Tucker, R.D., Osberg, P.H., and Berry, H.N., IV (2001) The geology of part of Acadia and the nature of the Acadian orogeny across central and eastern Maine. American Journal of Science, 301, 205-260.

Vielzeuf, D., Baronnet, A., Perchuk, A.L., Laporte, D., and Baker, M.D. (2007) Calcium diffusivity in alumino-silicate garnets: an experimental and ATEM study. Contributions to Mineralogy and Petrology, 154, 153-170.

Viete, D.R., Hermann, J., Lister, G.S. and Stenhouse, I.R. (2011) The nature and origin of the Barrovian metamorphism, Scotland: Diffusion length scales in garnet and inferred time scales. Journal of the Geological Society of London, 168, 115-132.

Vogt, K., Dohmen, R., and Chakraborty, S. (2015) Fe-Mg diffusion in spinel: New experimental

data and a point defect based model. American Mineralogist, 100, in press.

Wheeler, J. (2014) Dramatic effects of stress on metamorphic reactions. Geology, 42, 647-650.

Wing, B.A., Ferry, J.M., and Harrison, T.M. (2003) Prograde destruction and formation of monazite and allanite during contact and regional metamorphism of pelites: petrology and geochronology. Contributions to Mineralogy and Petrology, 145, 228-250.

Zhang, Y., and Cherniak, D.J., Eds. (2010) Diffusion in Minerals and Melts, 72, 1038 p. Reviews in Mineralogy and Geochemistry, Mineralogical Society of America, Chantilly, Virginia.

FIGURE CAPTIONS

FIGURE 1. BSE images of ankerite grains with dolomite cores in representative samples from the study areas in Maine and Vermont. In all images the contact between the dolomite core and surrounding ankerite rim is sharp but irregular. Smaller more rounded dark areas in ankerite are quartz inclusions. Differences in greyscale brightness of ankerite correspond to differences in Fe/(Fe+Mg). Dol = dolomite, Ank = ankerite, Qz = quartz, Ms = muscovite, Pl = plagioclase, Ab = albite, Chl = chlorite. **a.** Marl sample 5-62 from the garnet zone, location 5, Maine (Fig. 2). White square outlines the area of NanoSIMS analysis across the dolomite-ankerite contact in Fig. 8c. **b.** Pelite sample 417A from the chlorite zone, location 417, Maine (Fig. 2). **c.** Marl sample 21-35I from the garnet zone, location 21-35, Vermont (Fig. 3). Narrow white rectangle identifies the area in which the profile in BSE greyscale in Fig. 9d was measured across the dolomite-ankerite contact with a FEG-SEM. **d.** Marl sample Q1j from the biotite zone, location Q1, Vermont (Fig. 3) White square outlines the area of NanoSIMS analysis across the dolomite-ankerite contact in Fig. 8d. **e.** Psammite sample NHd1I from the chlorite zone, location NHd1, Vermont (Fig. 3). **f.** Pelite sample NHd1K from the chlorite zone, location NHd1, Vermont (Fig. 3).

FIGURE 2. Sketch map of the geological setting of the Waterville-Vassalboro area, Maine (after Osberg 1968, 1979, 1988, and Ferry, 1984). Arrowheads point to the high-grade side of isograds. Sample locations are the same as those of Ferry (1994) and Penniston-Dorland and Ferry (2006). Symbols represent locations from which at least one ankerite-bearing sample was examined. Shapes of symbols refer to rock type (circles are marls; squares are pelites; stars are low-Al sulfide-rich schists). Filled symbols indicate that at least one sample of a given rock type contains ankerite grains with a dolomite core; unfilled symbols indicate that no dolomite cores were observed in samples of a given rock type. Black symbols identify locations where no sample of a given rock type contains biotite; red symbols indicate at least one sample of a given rock type contains biotite. Denominators of fractions indicate how many ankerite-bearing samples of a given rock type at a given location were examined (if more than one); numerators indicate in how many of those samples contain ankerite grains with a dolomite core.

FIGURE 3. Sketch map of the geological setting of the study area in east-central Vermont (after Lyons, 1955; Doll et al., 1961; Ferry, 1992, 1994). Arrowheads point to the high-grade side of isograds (B = biotite, K = kyanite). Western portion of the biotite isograd based on samples examined in this study rather than on Doll et al. (1961). Yellow pattern is the Albee Formation and Ammonoosuc Volcanics, undifferentiated. Symbols and fractions are the same as in Fig. 2. Diamonds and hexagons refer to psammites and metaigenous rocks, respectively. Green symbols indicate at least one sample of marl contains calcic amphibole and biotite. Key to sample locations in text, tables, and other figures: a = NHd1, b = Q1, c (inset) = 4-1, d = 21-18, e = 21-16, f = 21-35, g = 26-1, h = 26-8, i = 33-6, j (inset) = 48-30.

FIGURE 4. Measured range of Fe/(Fe+Mg) of ankerite in 30 samples from location 5, Maine (Fig. 2) that contain ankerite grains with a dolomite core. The range in Fe/(Fe+Mg) rules out a solvus relationship between the dolomite cores and surrounding ankerite rims.

FIGURE 5. Relationship between Fe/Mg in ankerite and Fe/Mg in coexisting biotite (**a**) and chlorite (**b**) for selected samples that contain ankerite grains with a dolomite core from both the Waterville Formation (Maine) and Waits River Formation (Vermont). Diamonds are dolomite-phlogopite pairs in 14 samples from four contact aureoles (Davis and Ferry, 1993; Ferry, 1996; Ferry and Rumble, 1997; Ferry et al., 1998). Yellow band is the range in Fe/Mg for all analyzed dolomite cores in this study. Slopes of lines are identical within error of measurement to slopes determined from a larger data set of ankerite-biotite and ankerite-chlorite pairs from the Waterville and Waits River Formations (Penniston-Dorland and Ferry, 2006). The near-linear data arrays indicate that biotite and chlorite were in Fe-Mg exchange equilibrium (or nearly so) during regional metamorphism with ankerite rims but not with the dolomite cores.

FIGURE 6. Distribution of samples containing ankerite grains with dolomite cores (solid lines) and samples containing only ankerite grains without dolomite cores (dashed lines) as a function rock type and metamorphic grade (defined by standard index minerals in pelitic schists). Colors distinguish the study areas in Maine (black) and Vermont (red). Both ankerite and dolomite cores disappear together with increasing grade in Maine. Samples containing only ankerite grains without dolomite cores persist to higher grades in Vermont than do ankerite grains with dolomite cores.

FIGURE 7. BSE images illustrating the increase in grain size of ankerite, quartz, and calcite with increasing grade of metamorphism in the study area in Vermont (Fig. 3). Mineral abbreviations

are the same as in Fig. 1; DC = dolomite core. (**a**) Marl sample 26-8A, location 26-8 in the chlorite zone. (b) Marl sample 21-18A, location 21-18 in the kyanite zone. None of the ankerite grains in sample 21-18A contain a dolomite core.

FIGURE 8. (**a**) BSE image illustrating the petrographic context of NanoSIMS and TEM analyses of Fe/Mg across the contact between a dolomite core and surrounding ankerite rim in marl sample 21-35D, location 21-35 in the garnet zone, Vermont (Fig. 3). White square identifies the area analyzed by NanoSIMS. Narrow white rectangle identifies the area from which a TEM foil was removed using a FIB instrument. Mineral abbreviations are the same as in Fig. 1. (**b**) Measured NanoSIMS profile in Fe/Mg (black circles) perpendicular to the dolomite-ankerite contact in panel a. (**c**) Measured NanoSIMS profile in Fe/Mg perpendicular to the same dolomite-ankerite contact in Fig. 1a of marl sample 5-62, location 5 in the garnet zone, Maine (Fig. 2). (**d**) Measured NanoSIMS profile in Fe/Mg perpendicular to the same dolomite-ankerite contact in Fig. 1d of marl sample Q1j, location Q1 in the biotite zone, Vermont (Fig. 3). In panels b-d, the red curve is a fit of the diffusion model described in the text to the profile; the best-fit values of Dt and $\sqrt{(Dt)}$ are given in the inset. The ion beam diameter in each case is larger than the retrieved value of $\sqrt{(Dt)}$. The profiles in samples Q1j and 5-62 yield the lowest and highest values of Dt from all eleven grains analyzed by NanoSIMS in this study.

FIGURE 9. (**a**) Bright-field TEM image of the foil extracted from the ankerite grain in Fig. 8a. The length of the foil is 12.4 μm, and the thickness (perpendicular to the plane of the image) is ~100 nm. Faint gray spots are where EDS analyses of Fe/Mg were performed along six traverses. The ends of the traverses are indicated by the black, red, and white circles and rings. Traverse 1 is in dolomite, traverse 2 is in ankerite, and the dolomite-ankerite contact is located

approximately halfway along traverses 3-6 and perpendicular to traverses 5 and 6. Black arrows point to the dolomite-ankerite contact interval along traverses 5 and 6. (**b**) Profiles in Fe/Mg measured by EDS using a FEG-TEM across the dolomite-ankerite contact along traverses 5 and 6 in panel a. Beam diameter is approximately the same size as the circles. Note the slight increase in Fe/Mg in ankerite near the dolomite-ankerite contact. Black arrows point to measured compositions at the dolomite-ankerite contact at the locations identified by the black arrows in panel a. (**c**) Profile in Fe/Mg along traverse 5 in panels a and b. Beam diameter is approximately the same size as the circles. The red curve is a fit of the diffusion model described in the text to the profile; the best-fit values of Dt and $\sqrt{(Dt)}$ are given in the inset. The ion beam diameter is slightly larger than the retrieved value of $\sqrt{(Dt)}$. (**d**) Greyscale profile measured using a FEG-SEM perpendicular to the contact between dolomite core and ankerite rim in a grain in sample 21-35I, location 21-35 in the garnet zone, Vermont (Figs. 1c, 3). Beam diameter is approximately the same size as the circles. The solid red curve is a fit of the diffusion model described in the text to the profile; the best-fit values of Dt and $\sqrt{(Dt)}$ are given in the inset. The dashed red lines are for values of Dt a factor of 5 greater than and less than the best-fit value. The ion beam diameter is smaller than the retrieved value of $\sqrt{(Dt)}$.

FIGURE 10. Temperature-oxygen activity (a_{O_2}) conditions of the experiments by Müller et al. (2012) and during metamorphism in Maine and Vermont. For reference, HM is the hematite-magnetite buffer, and QFM is the quartz-fayalite-magnetite buffer. Curves calculated from thermodynamic data in Holland and Powell (1998) and from O_2 fugacities derived from the CORK equation-of-state of Holland and Powell (1991). Oxygen activity referenced to pure O_2 at P and T of interest. Black curves are for P = 0.1 MPa. In bar units of pressure, at P = 1, $a_{O_2} = f_{O_2} = X_{O_2}$, where f is fugacity and X is mole fraction. Black curves for $CO_2 = 2\ CO + O_2$ and $CO_2 =$

$C + O_2$ assume $a_{CO_2} = 1$ (the latter a fictive equilibrium). For the graphite-CO_2 equilibrium, the red band includes corrections to the corresponding black curve for the range of $P = 350 – 800$ MPa and $a_{O_2} = 0.099 – 0.362$ during metamorphism in the biotite and garnet zones in Maine and Vermont (Figs. 2, 3). The P correction for metamorphism (< 0.2 log units) is barely discernable at the scale of the figure. Values of a_{CO_2} during metamorphism were calculated from equilibrium 6 in the text. Oxygen activity differs by 17 – 20 orders of magnitude between the experiments and the conditions of metamorphism of samples from the biotite and garnet zones of Maine and Vermont at which ankerite grains with dolomite cores are preserved.

This is a preprint, the final version is subject to change, of the American Mineralogist (MSA)
Cite as Authors (Year) Title. American Mineralogist, in press.
(DOI will not work until issue is live.) DOI: http://dx.doi.org/10.2138/am-2015-5209

Ferry et al. -- Fig. 1

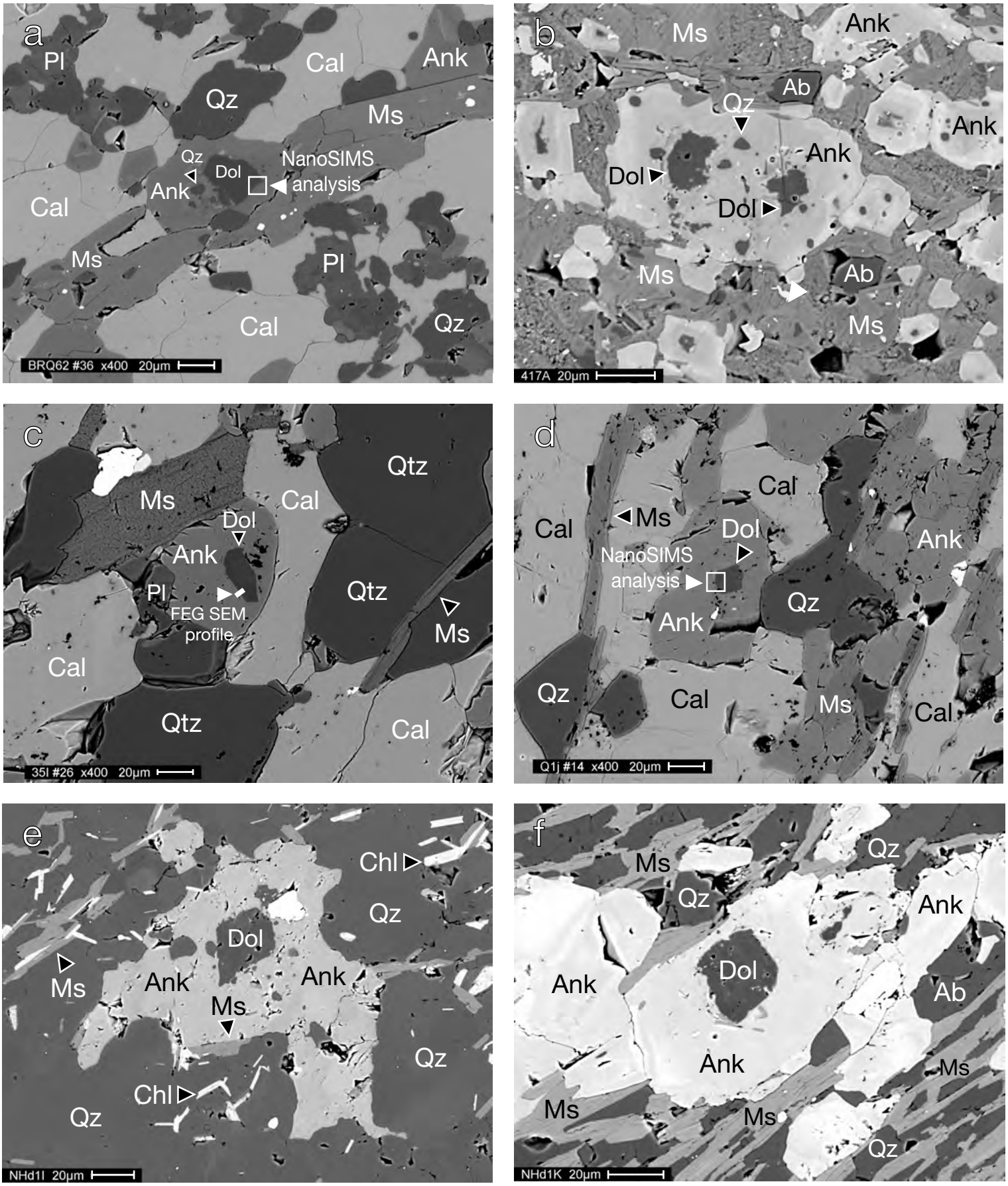

This is a preprint, the final version is subject to change, of the American Mineralogist (MSA)
Cite as Authors (Year) Title. American Mineralogist, in press.
(DOI will not work until issue is live.) DOI: http://dx.doi.org/10.2138/am-2015-5209

Ferry et al. -- Fig. 2

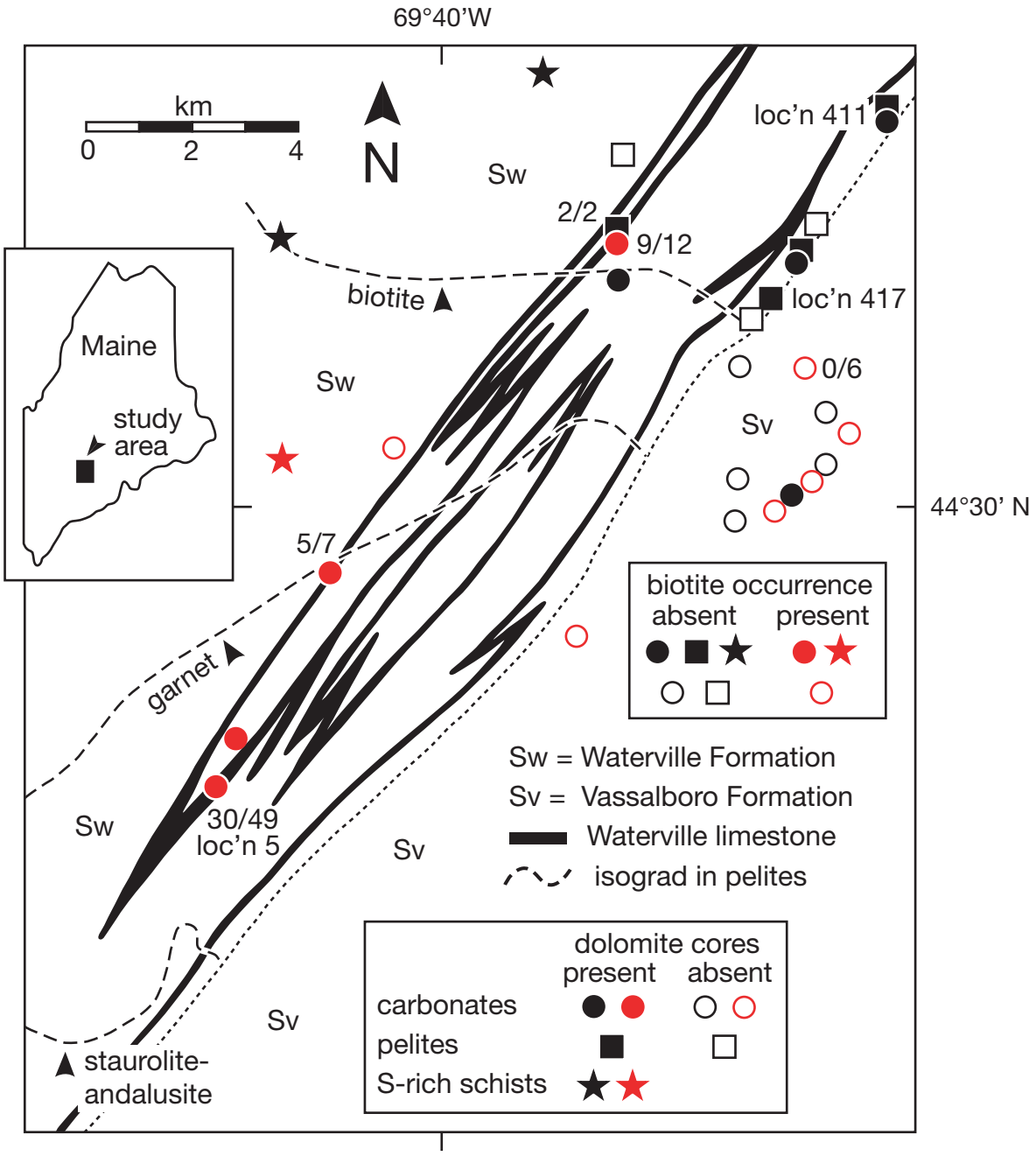

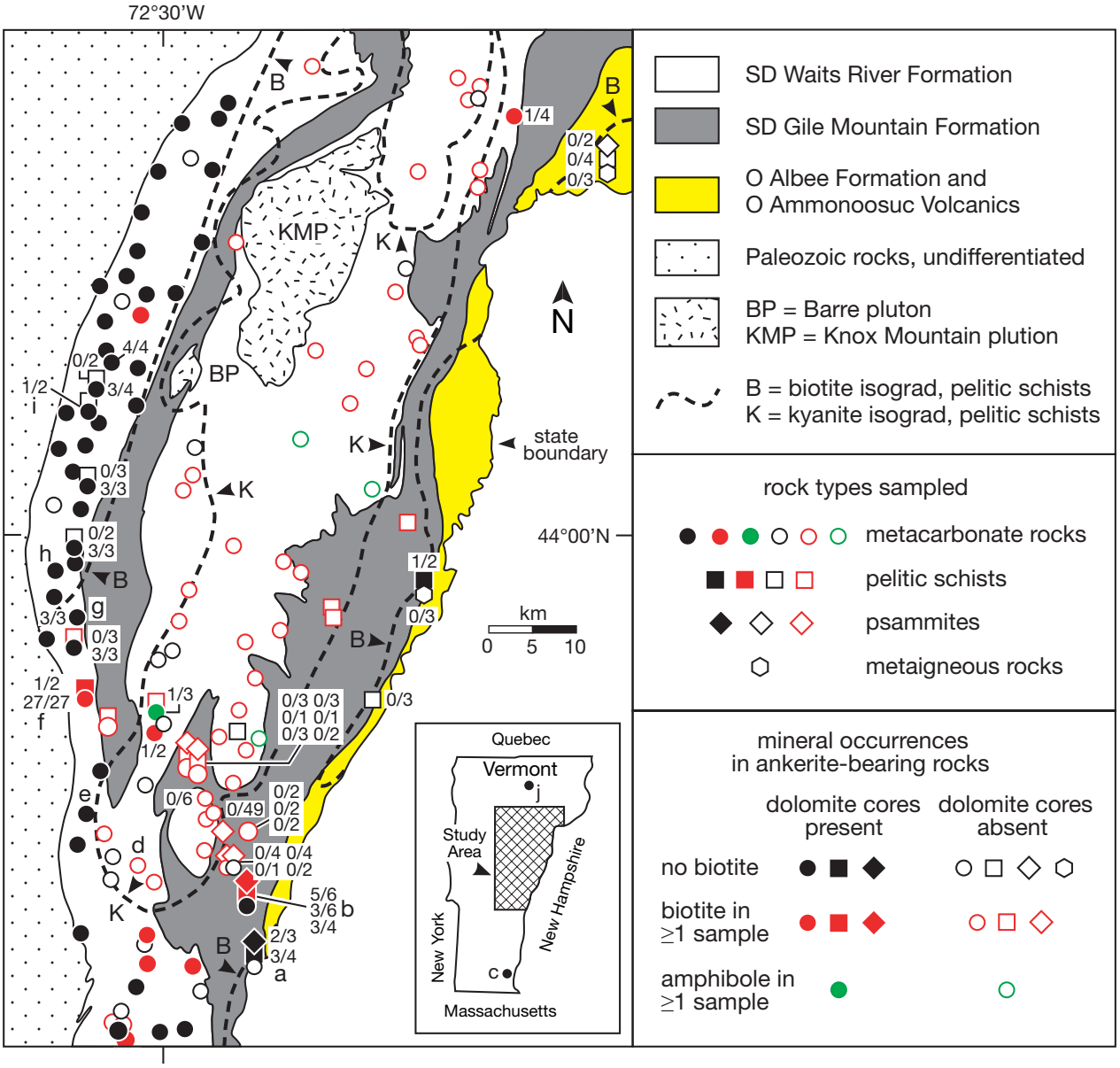

Ferry et al. -- Fig. 3

Ferry et al. -- Fig. 4

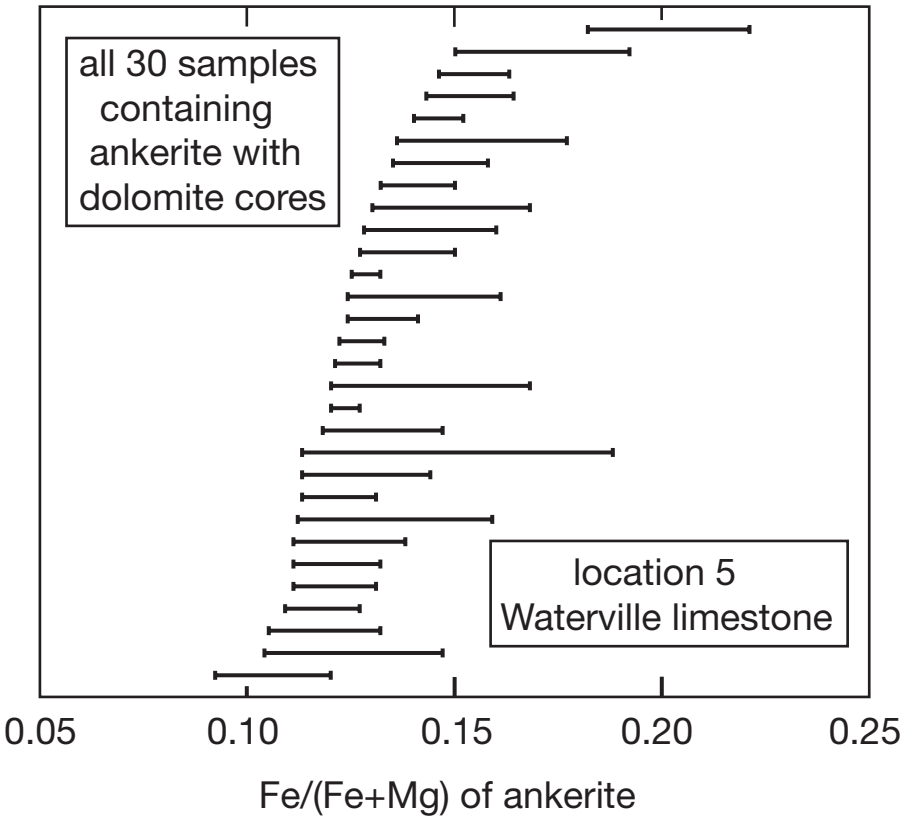

Ferry et al. -- Fig. 5

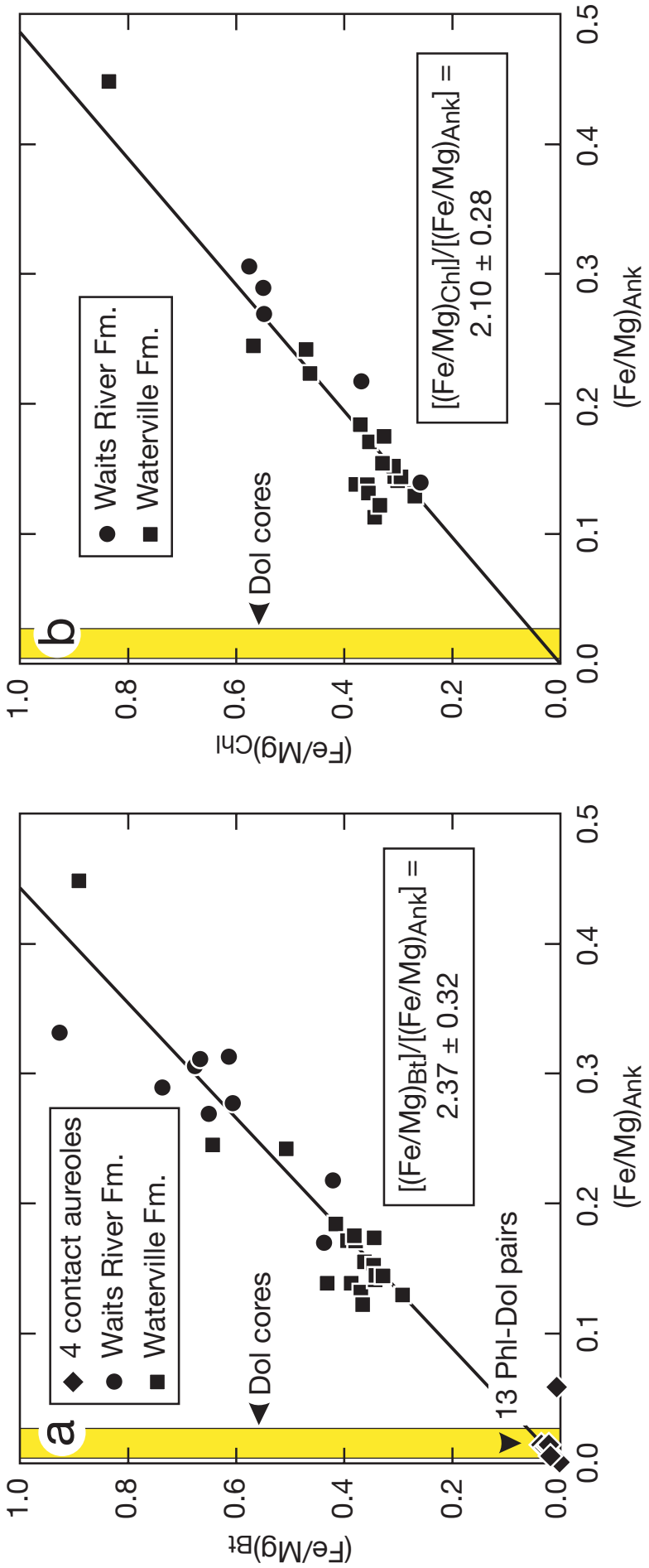

Ferry et al. -- Fig. 6

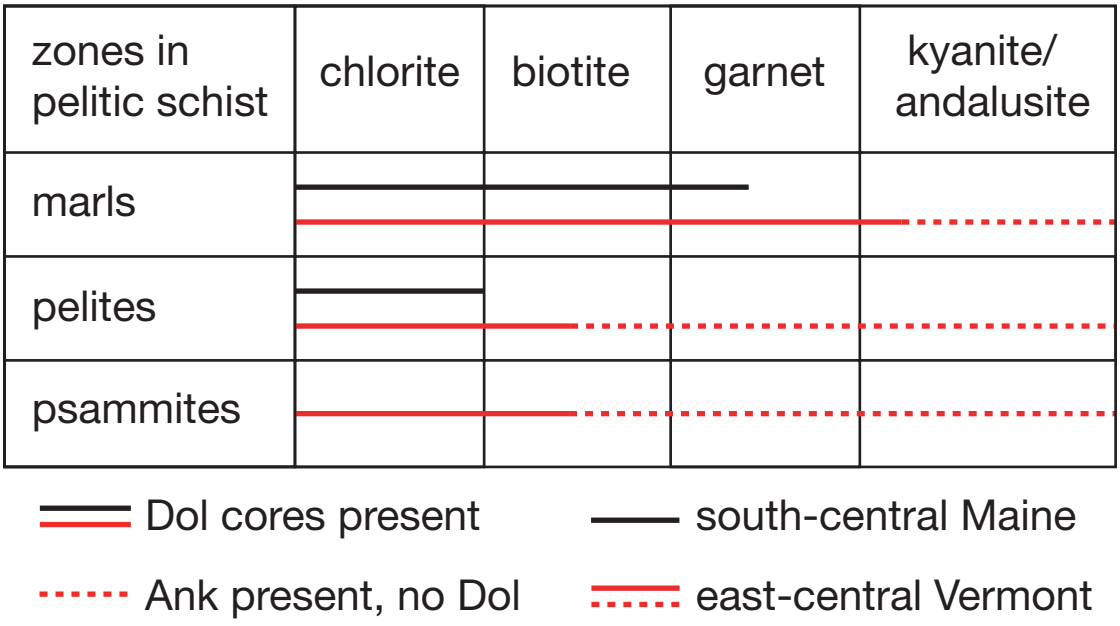

Ferry et al. -- Fig. 7

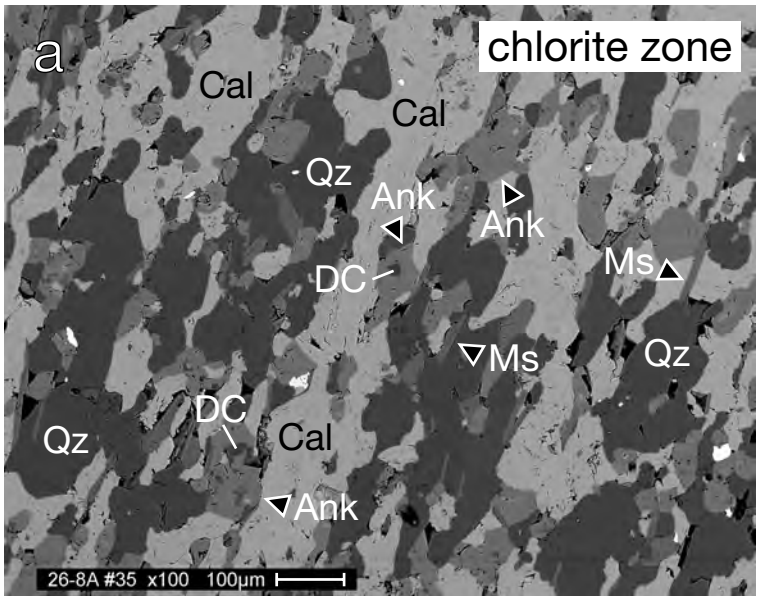

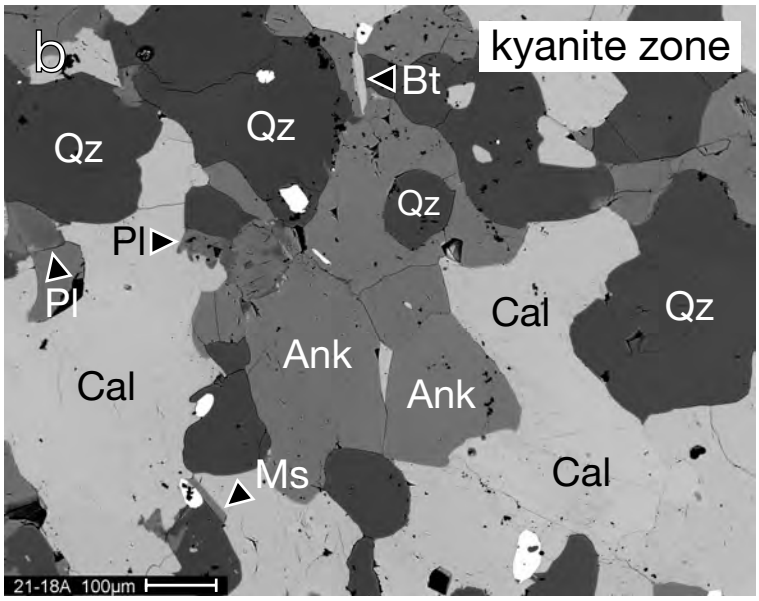

Ferry et al. -- Fig. 8

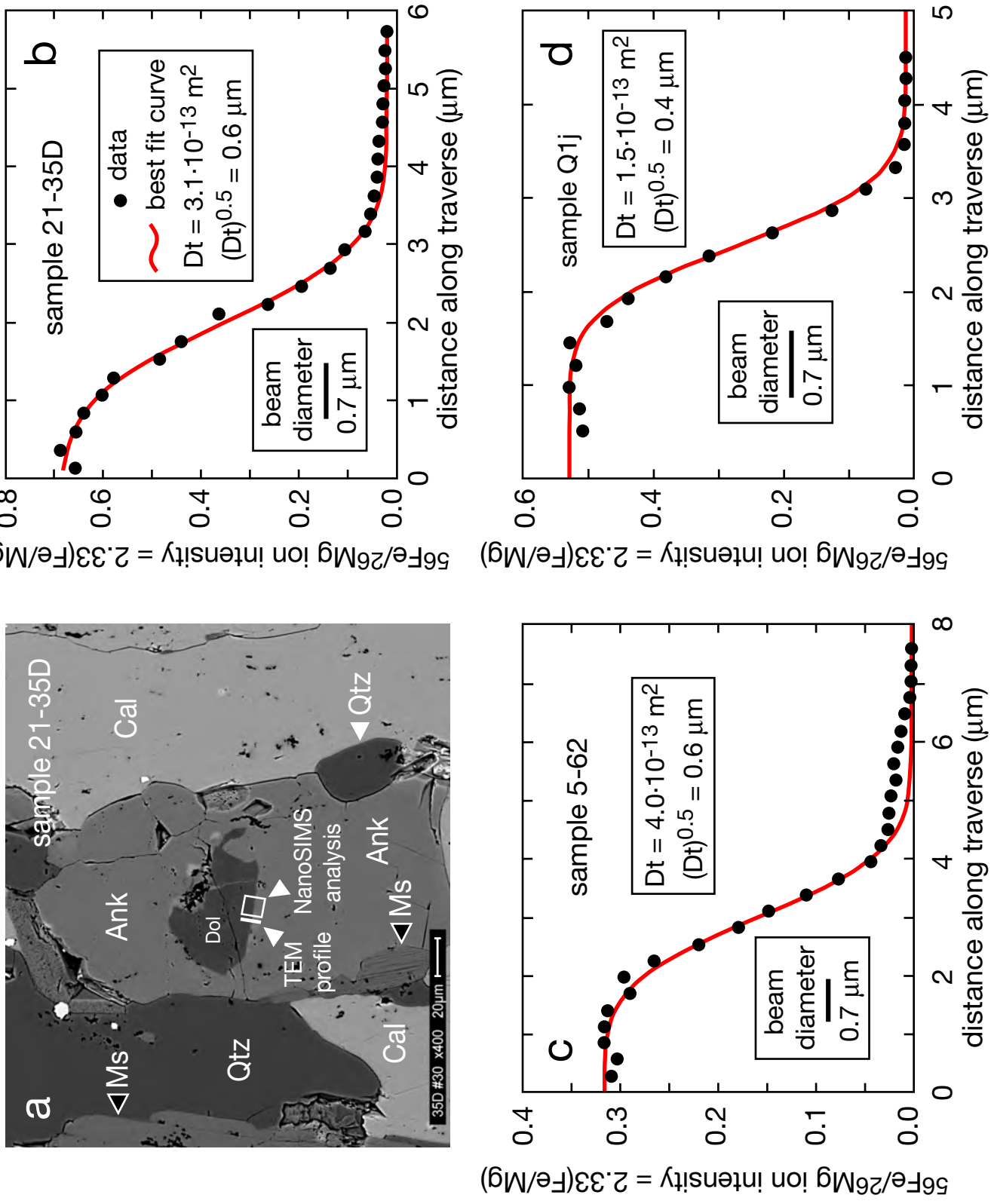

This is a preprint, the final version is subject to change, of the American Mineralogist (MSA)
Cite as Authors (Year) Title. American Mineralogist, in press.
(DOI will not work until issue is live.) DOI: http://dx.doi.org/10.2138/am-2015-5209

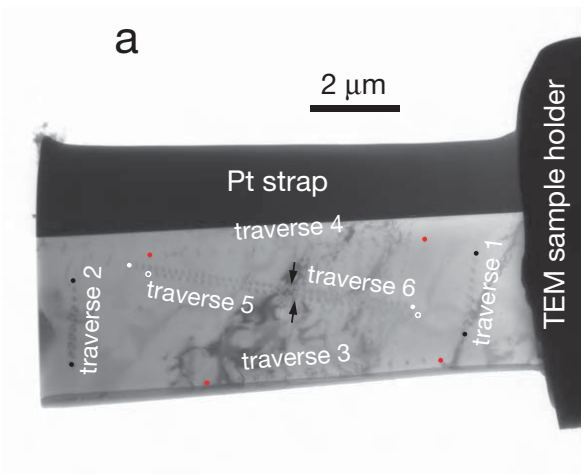

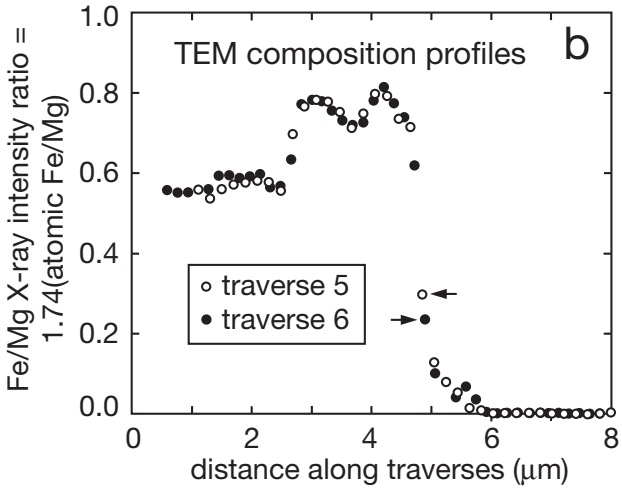

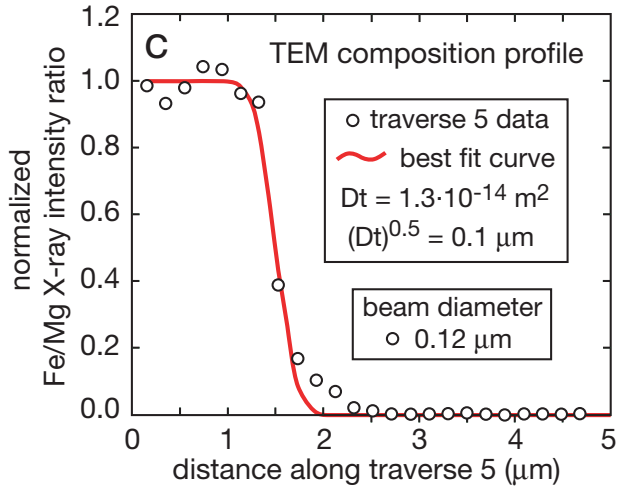

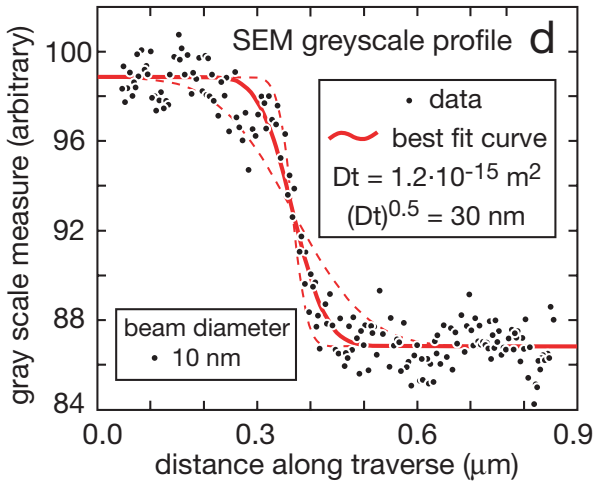

Ferry et al. -- Fig. 9

Ferry et al. -- Fig. 10

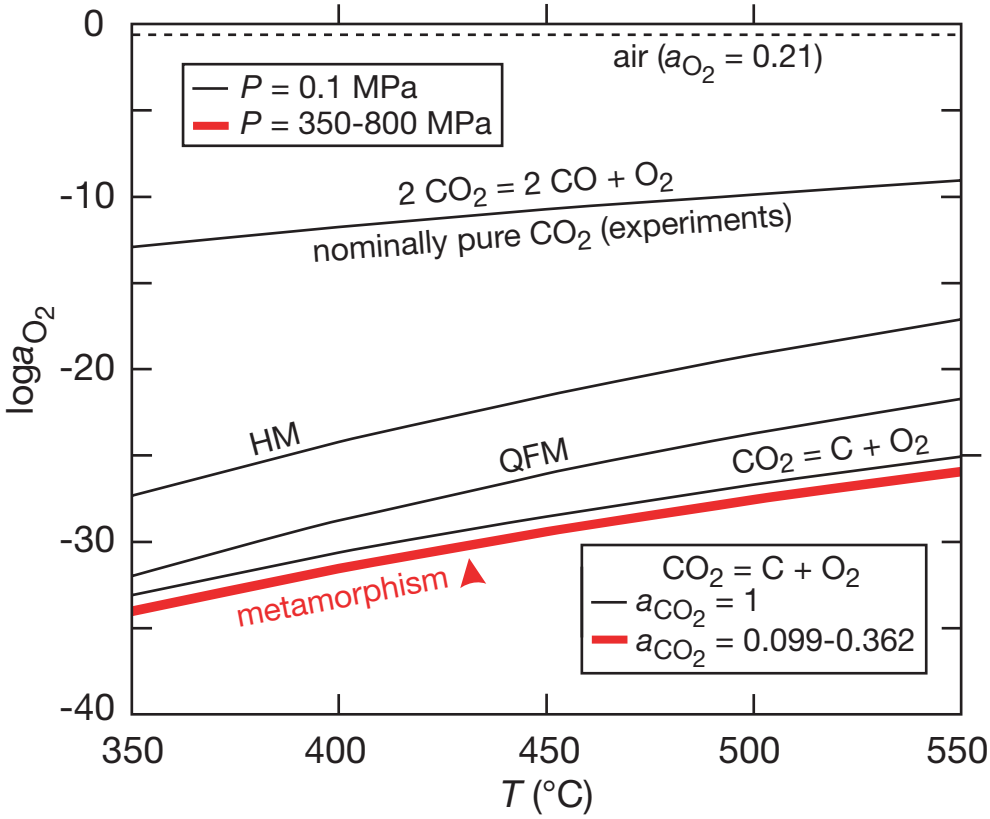

Table 1. Compositions of ankerite and dolomite cores in selected samples of marl

Sample	5-62	5-62	Q1D	Q1D	Q1j	Q1j	4-1A	4-1A	21-16A	21-16A
Formation[a]	Swls	Swls	SDgm	SDgm	SDgm	SDgm	SDwr	SDwr	SDwr	SDwr
Map[b]	F2/L5	F2/L5	F3/Lb	F3/Lb	F3/Lb	F3/Lb	F3I/Lc	F3I/Lc	F3/Le	F3/Le
Mineral	ankerite	dolomite	ankerite	dolomite	ankerite	dolomite	ankerite	dolomite	ankerite	dolomite
Ca[c]	1.024	1.016	1.017	1.024	1.028	1.023	1.017	1.029	1.025	1.048
Mg[c]	0.802	0.978	0.695	0.942	0.724	0.962	0.749	0.959	0.656	0.934
Fe[c]	0.157	0.006	0.242	0.026	0.206	0.011	0.217	0.011	0.299	0.016
Mn[c]	0.017	0.001	0.045	0.008	0.042	0.003	0.018	0.001	0.020	0.001
Avg. X_{Fe}[d]	0.163	0.006	0.258	0.027	0.222	0.011	0.225	0.011	0.313	.017
Range X_{Fe}[d]	0.16-0.17	<0.01	0.25-0.26	0.02-0.03	0.20-0.23	0.01	0.19-0.25	0.00-0.02	0.31-0.32	0.01-0.02
oxide sum[e]	100.08	100.40	100.29	100.32	100.16	99.94	100.08	100.24	100.30	99.69

Sample	21-35D	21-35D	21-35I	21-35I	26-1C	26-1C	33-6B	33-6B	48-30-8	48-30-8
Formation[a]	SDwr	SDwr	SDwr	SDwr	SDwr	SDwr	SDwr	SDwr	SDwr	SDwr
Map[b]	F3/Lf	F3/Lf	F3/Lf	F3/Lf	F3/Lg	F3/Lg	F3/Li	F3/Li	F3I/Lj	F3I/Lj
Mineral	ankerite	dolomite	ankerite	dolomite	ankerite	dolomite	ankerite	dolomite	ankerite	dolomite
Ca[c]	1.028	1.061	1.029	1.040	1.008	1.036	1.002	1.036	1.020	1.032
Mg[c]	0.751	0.933	0.740	0.943	0.833	0.956	0.780	0.953	0.877	0.963
Fe[c]	0.206	0.006	0.216	0.014	0.151	0.008	0.212	0.010	0.101	0.004
Mn[c]	0.015	0.000	0.014	0.002	0.007	0.001	0.007	0.001	0.002	0.001
Avg. X_{Fe}[d]	0.216	0.006	0.226	0.015	0.153	0.008	0.213	0.010	0.104	0.004
Range X_{Fe}[d]	0.21-0.22	<0.01	0.22-0.23	0.01-0.03	0.15-0.16	0.00-0.02	0.21-0.23	0.01-0.02	0.10-0.11	<0.01
oxide sum[e]	100.32	100.68	100.09	100.42	99.88	100.17	100.31	100.15	100.10	100.21

[a]Swls is the limestone member of Waterville Formation; SDgm is the Gile Mountain Formation; SDwr is the Waits River Formation.

[b]Figure/Location number or letter. “F3I” refers to the inset map in Fig. 3.

[c]Cations per 2 total cations, excluding C.

[d]X_{Fe} = Fe/(Fe+Mg).

[e]Oxide sum assuming stoichiometric CO_2.

Table 2. Occurrence of dolomite cores in ankerite organized by rock type and presence or absence of biotite

Rock type	Biotite occurrence	Waterville Formation, ME	Vassalboro Formation, ME	Waits River Formation, VT	Gile Mountain Formation, VT	Albee Formation, VT
Marl	Absent	17/21 = 81%	1/8 = 13%	121/144 = 84%	3/9 = 33%	none
Marl	Present	30/51 = 59%	0/8 = 0%	16/122 = 13%	0/7 = 0%	none
Pelite	Absent	4/7 = 57%	not examined	0/8 = 0%	4/9 = 44%	0/4 = 0%
Pelite	Present	none	not examined	1/6 = 17%	3/14 = 21%	no ankerite
Psammite	Absent	not examined	not examined	none	2/3 = 67%	0/2 = 0%
Psammite	Present	not examined	not examined	none	5/20 = 25%	no ankerite

Note: Denominator of each fraction is the total number of samples examined with ankerite; numerator is the number of samples in which one or more ankerite grain has a dolomite core.

Table 3. Constraints on the duration (*t*) of metamorphic processes in years

	Peak *T* (°C)	NanoSIMS data	FEG-TEM data	FEG-SEM data
Measured *Dt* (m^2)		$(1.5\text{-}4.0)\cdot10^{-13}$	$1.3\cdot10^{-14}$	$1.2\cdot10^{-15}$
t residence at peak *T*	500	10-27	0.9	0.08
t residence at peak *T*	400	23-61	2.0	0.2
t, linear cooling[a]	500	37-101	3.3	0.3
t, linear cooling[a]	400	79-212	6.9	0.6
t, linear heating+cooling[b]	500	37-101	3.3	0.3
t, linear heating+cooling[b]	400	79-212	6.9	0.6

[a]Cooling from peak *T* to 100 °C.

[b]Heating from 100 °C to peak *T* immediately followed by cooling to 100 °C.